CHAPTER V

W49 A

5.1 Literature Reviews

The Giant Molecular Cloud (GMC), W49, is located in the constellation of Aquila at l=43.17°, b=+0.00° at a distance of 11.4±1.2 kpc (Gwinn et al., 1992). It is the most massive GMC in the Galaxy outside the Galactic centre with a mass of 10^6 $M_\odot$ and extending over more than 50 pc in diameter (Simon et al., 2001). Its radio emission comprises a radio continuum thermal source to the west, W49 A, and a non thermal source, W49 B, ~12′ to the east. W49 B has been identified as a supernova remnant (Mezger et al., 1967; Shaver and Goss, 1970), and W49 A as an active star-forming region. Embedded within W49 A is one of the brightest Galactic giant radio HII regions (10^7 $L_\odot$, Smith et al., 1978). It contains ~ 40 Ultra-Compact HII (UCHII) regions (de Pree et al., 1997; Smith et al., 2000) associated with a minimum of 40 central stars earlier than B3. There are three main IR peaks, defining three sub-regions: W49 SW (some papers have referred to this as W49, but in this thesis it will be referred to as W49 SW), W49 SE (commonly referred to as W49 S), and the strongest, W49 NW (more commonly referred to as W49 N; Harvey et al., 1977). W49 N contains the brightest HII regions, including a ring of UCHII regions, (defined as the "Welch ring" (Welch et al. 1987) and hot cores (Wilner et al. 2001Miyawaki et al., 2002). Figure 5.1 shows the three sub-regions. The brightest UCHII component, G (e.g. Dreher et al., 1984; de Pree et al., 1997), and the strongest H_2O masers in the Galaxy (Walker et al. 1982) are to be found in W49 N. W49 S is a "cometary" UCHII region (Wood et al. 1989) located ~ 2′ southeast of W49 N. W49 SW is on the southwest of W49 N.

Figure 5.2, taken from McGrath et al. (2004), shows the 3.6 cm radio continuum image of the entire W49 A complex. The H II regions where maser activity is prominent- W49 N - are indicated. These regions are shown in more detail in the inset 1.3 cm continuum images. The H II region, G1/G2, is the main source of water masers in W49 N, together with a smaller cluster of H_2O masers located close to the H II region B1/B2. The H_2O masers in W49 N are known to be the most luminous in the Galaxy and their velocity distribution is known to span at least 560 km s^{-1} (Walker et al. 1982). Homeier and Alves (2005), using the SOFI near-infrared camera, have estimated a total stellar mass of ~5-7 $\times 10^4 M_\odot$ in W49 A. It has also been shown the phenomenon of sub-clustering is essential for a description of star formation in the W49 A molecular cloud, at least as traced by the massive stars. Smith et al. (2009) have used Michelle1 [1] on the Gemini North telescope to observe W49 N. They have proposed a CO outflow model in which

[1]Michelle is a mid-infrared (7-26 micron) imager and spectrometer, formerly in use at UKIRT but now on long-term loan at Gemini.

the origin of the outflow is in region G. The red-shifted wing is in a northwest direction and the blue-shifted wing is to the southeast. The orientation of the CO outflow and ionized cavities is orthogonal to the water maser outflow (the small white arrows in Figure 5.3). It could be that the water maser outflows trace dense material in an equatorial torus or envelope, or they may originate at the interface between the cavity and disc envelope close to the source (Mac Low et al., 1994). A similar orientation is seen in S140-IRS1 (Hoare, 2006).

5.2 OH Masers in W49 A

W49 A has been observed in the four ground-state OH spectral line transitions at 1.6 GHz and in two of the excited state ones at 6.0 GHz. No signal has been detected in the current observations at 6030 MHz and 6035 MHz down to an upper limit of 18 mJy beam^{-1}. The calibrated spectra for the two main lines at 1665 and 1667 MHz are shown in Figures 5.4 and Figure 5.5 respectively. Since results of observations of the satellite lines at 1612 MHz and 1720 MHz have not been published in the earlier work of Argon et al. (2000), the results and discussion presented hereafter will concentrate on the OH maser emission from these two lines.

The satellite-line transitions in W49 A were observed by MERLIN on 2005 May 5-10. The main observational details are given in Chapter 3, Table 3.2. The results will be presented for the three sub-regions, W49 SW, W49 S and W49 N.

5.3 W49 S

The distribution of the OH masers in this sub-region is presented in Section 5.3.1 and their kinematics are presented in Section 5.3.2. The polarization of the maser features are presented in Section 5.3.3. Magnetic fields derived from Zeeman measurements are presented in Section 5.3.4.

5.3.1 OH Maser Distribution

Elliptical Gaussian components have been fitted to the emission in those frequency channels in which the emission levels satisfy the criteria for the measurement of intensities and positions described in Chapter 3, Section 3.7.2. There are usually one or at most three components in each channel map, with the individual components being unresolved. The rmsnoise level (σ_{rms}) in most of the channel images is ~ 8 mJy beam^{-1}, with the noise level being up to a maximum of $\sim 0.5\%$ of the peak flux in those channels with visible emission. The position and peak flux of each component have been measured as described in Chapter 3, Section 3.7.2 and components in successive channels then assigned as features. The results for the circularly polarised emission are summarized in Table 5.1, which

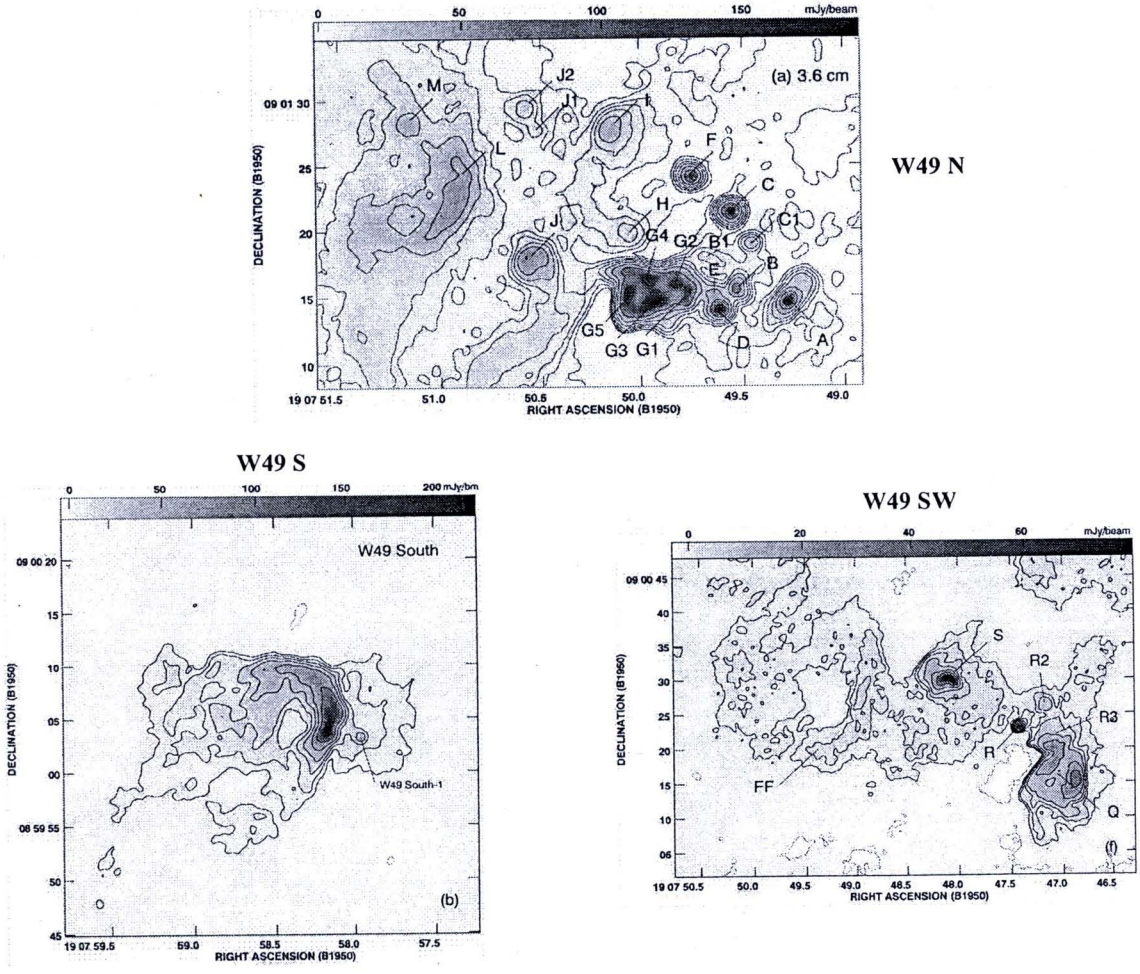

Figure 5.1 This figure has been taken and modified from de Pree et al. (1997). It shows the 3.6 cm radio-continuum contours (and in grey-scale) of the W49 A region. The beam, θ_{beam}=0.8″.

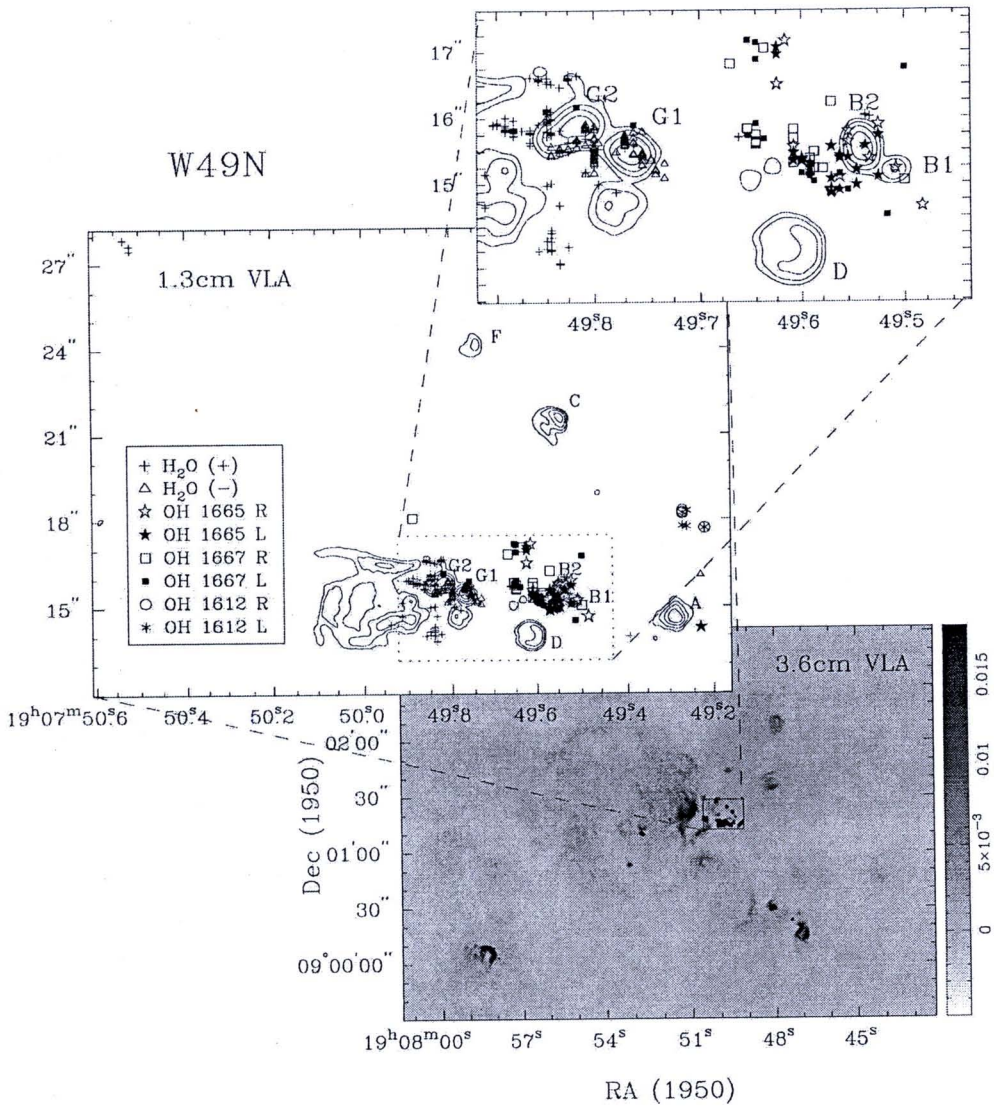

Figure 5.2 Overview image of W49 N continuum at 3.6 cm (from de Pree et al. 1997) and 1.3cm insets (from de Pree et al. 2000). Beam size for the 3.6cm continuum is 0.″80 × 0.″78, PA = −63°. Beam size for the 1.3cm continuum is 0.28 × 0.″24, PA = 8°. Contours are at 10, 20, 40, 80, and 160 mJy beam^{-1}. H_2O and OH masers (from Argon et al. 2000) are over-plotted on the 1.3cm continuum. H_2O masers with positive (negative) velocities with respect to the LSR are represented by crosses (triangles), while OH masers are denoted in the key by their transition (in MHz) with an R (L) for right (left) circularly polarized masers. Absolute alignment between the H_2O and OH maser positions is limited by the absolute positional accuracy of the OH masers (∼0.″3). The alignment between the H_2O masers and the 1.3 cm continuum has an rms error of 0.″01.

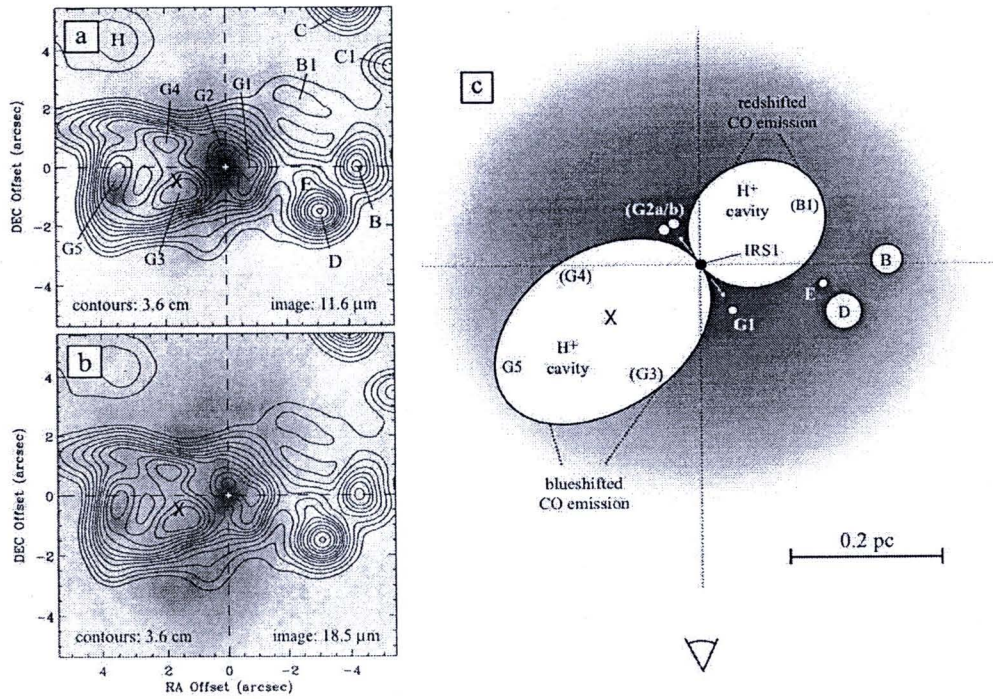

Figure 5.3 This figure is taken from Smith et al. (2009). Contours of 3.6 cm radio continuum superposed over the Gemini/Michelle images of source G at 11.6 μm (a) and 18.5 μm (b). (c) A cartoon of one possible geometric model for source G and its environment, viewed from the north (an Earth-based observer is at the bottom of the drawing). Features which are well above or below the plane of the drawing are in parentheses. The walls of the large cavities give rise to the blueshifted and redshifted CO outflow to the east and west, respectively (Scoville et al. 1986), while the white arrows in the equatorial plane denote the approximate zones where the H_2O masers are found. The 'X' marks the spot associated with the approximate peak and centroid of hard X-ray emission detected recently by Tsujimoto et al. (2006).

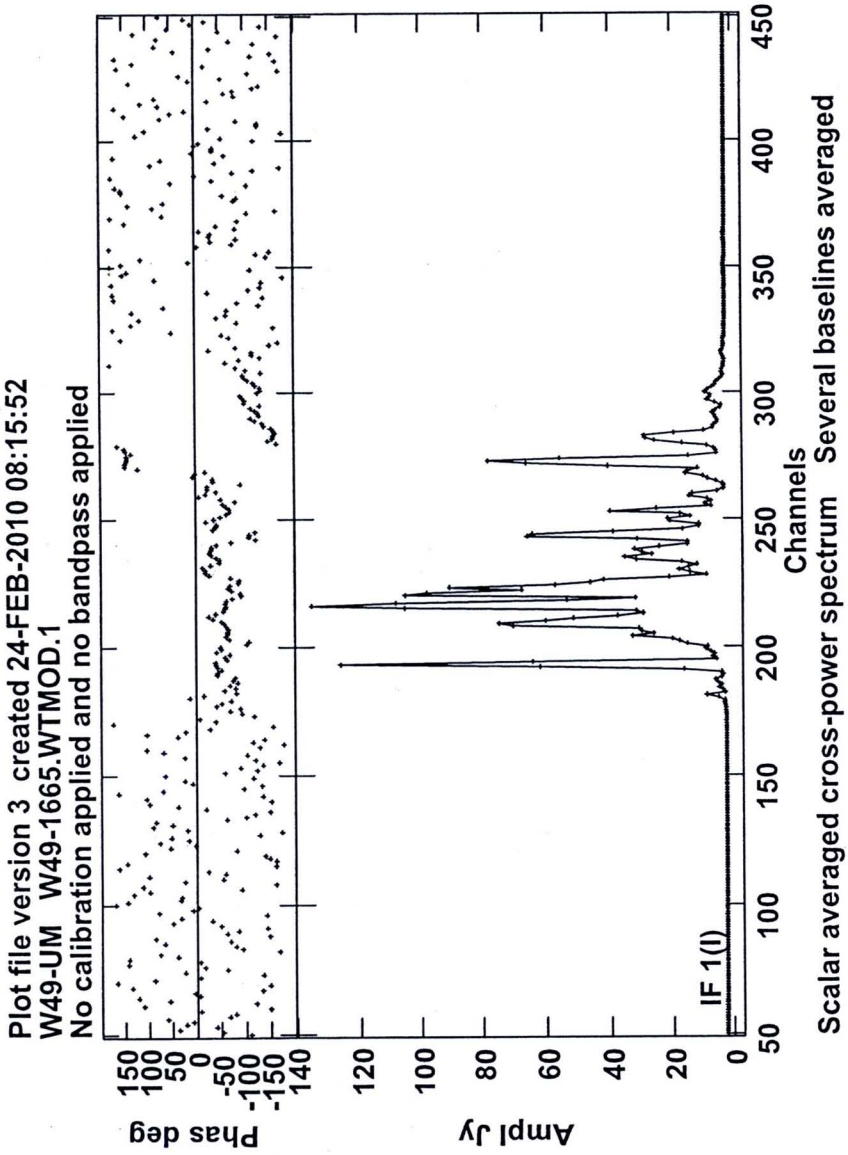

Figure 5.4 Scalar averaged cross-power spectrum of 1665 OH maser towards W49 A.

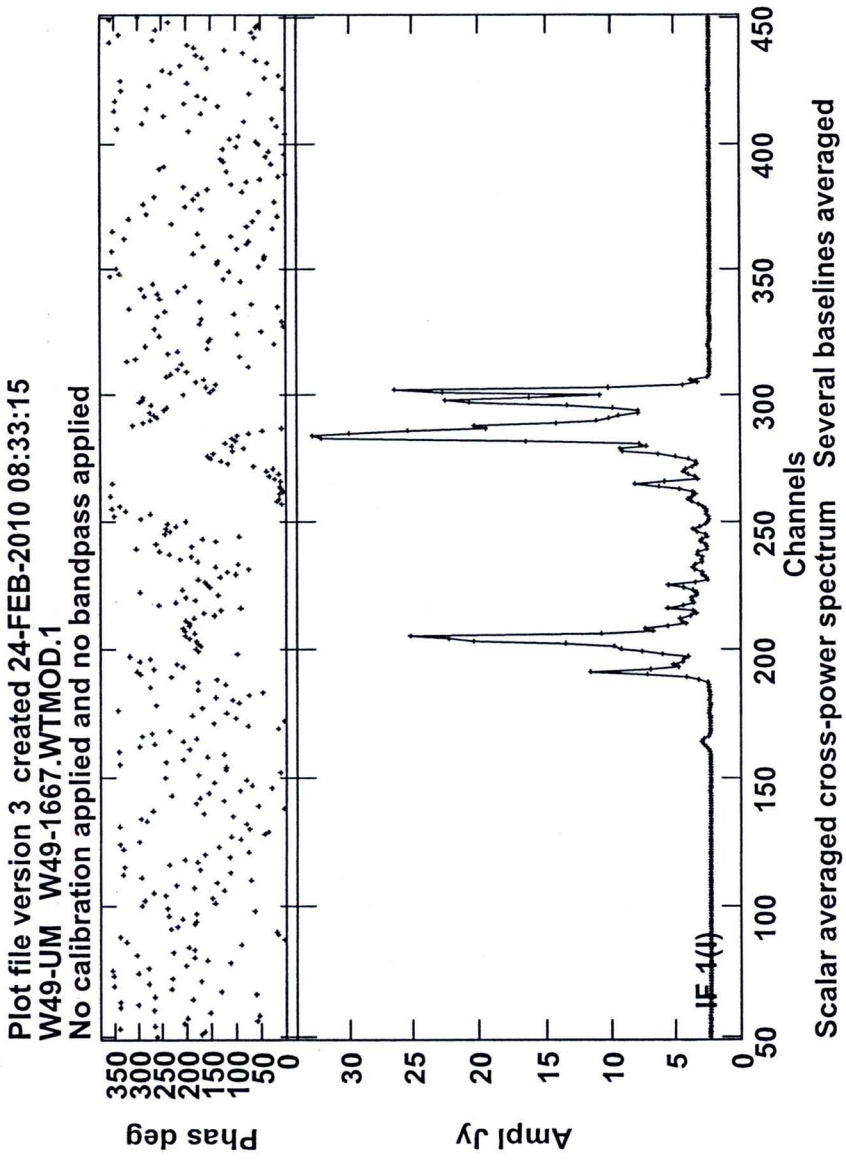

Figure 5.5 Scalar averaged cross-power spectrum of 1667 OH maser towards W49 A.

shows the velocity, position, position uncertainty and peak flux density of each circularly polarized OH maser. The positional uncertainties in each feature have been calculated from the standard deviation of the position of the components in that particular feature. The maps and plots presented in Figure 5.8 - Figure 5.13 and Figure 5.13 show positions relative to the pointing position for W49 S as shown in Table 1 of Argon et al. (2000); R.A.(J2000)=$19^h10^m21^s.65$, Dec.(J2000)=+09° 05′ 02″.6.

Table 5.1 shows the 10 different spectral line features, six of which are seen in left circular polarization (LCP) and seven in right circular polarization (RCP), which have been deteced at 1612 MHz. At 1720 MHz, 7 spectral line features are seen, four in LCP and three in RCP. The velocity profiles of the 1612 and 1720 MHz OH maser features are shown in Figures 5.6 and 5.7 respectively. All the OH maser emission at 1612 MHz and 1720 MHz is limited to a velocity range from 12 to 22 km s^{-1}.

Figure 5.8 shows the positions of the 1612 and 1720 MHz OH maser features found in these observations, superimposed on the 8.4 GHz continuum map of Argon et al. (2000). The black symbols represent the results from the earlier work and the current results are represented by the coloured circle symbols. Almost all the OH masers have positions which nearly match those of the earlier work. W49 S has been defined as belonging to the cometary class of compact HII regions, since the emission is dominated by a bright "head" component (280 Jy at 1720 MHz), with a diffuse "tail" trailing towards the southeast. Moreover, the parabolic distribution of the OH masers around the central region is strong evidence for a bow shock which has been proposed by Vanburen et al. (1990) and Mac Low et al. (1991). A number of OH maser features appear to be blending at the same positions, especially at (0.5,-0.3) aresec. This agrees well with de Pree et al. (1997), who note that there are one or more compact sources embedded in the dense molecular material on the edge-brightened side. The expansion of an ionization front (and the compression wave that precedes it; see Garcia-Segura and Franco, 1996) may be responsible for triggering the star formation in the dense molecular cores. One new group has been found approximately 4 arcsec to the south-west of the head of the cometary HII region. This group might belong to 'W49 South-l', which has been defined by de Pree et al. (1997).

5.3.2 OH Maser Kinematics

Figure 5.9 shows the position offsets from the pointing position and the velocities of the features in both circular polarizations. These plots compare well with the results taken from Argon et al. (2000), the masers appearing to be grouped into two clumps. The northern clump contains all of the features with velocities from 13.05 to 20.45 km s^{-1}, whereas the southern group contains all of the features with velocities in the range 12.99 to 13.99 km s^{-1}. The masers associated with the cometary shape exhibit a systematic gradient of velocity with position, the highest velocities to the north and the lowest velocities to the south as

Table 5.1 OH maser features in W49 S. For each frequency and polarization, flux weighted mean velocities and positions are given for each feature. The positions are given relative to (0,0) at R.A.(J2000)=$19^{h}10^{m}\ 21\overset{s}{.}65$, Dec.(J2000)=$+09°\ 05'02''.6$.

Feature	Stoke no.	Vel. (km/s)	RA offset (arcsec)	Dec offset (arcsec)	σ_{RA} (arcsec)	σ_{Dec} (arcsec)	Peak flux (Jy b^{-1})	I (Jy b^{-1})	Q (Jy b^{-1})	U (Jy b^{-1})	V (Jy b^{-1})	PA °	M_L (%)	M_C (%)	M_T (%)
1612-RCP :															
A	1	20.45	0.478	–0.370	0.005	0.005	0.14	0.07	0.00	–0.01	0.07	–	0.0	91.7	91.7
B	–	16.90	0.489	0.236	0.016	0.011	0.18	–	–	–	–	–	–	–	–
C	4	15.37	0.425	0.078	0.004	0.005	0.23	0.12	–0.02	0.00	0.10	–	0.0	84.4	84.4
D	5	13.93	0.723	–1.706	0.003	0.009	0.39	0.20	0.00	–0.01	0.17	–	0.0	87.2	87.2
E	7	13.24	0.743	–1.603	0.005	0.017	0.25	0.18	0.00	0.01	0.06	–	0.0	34.6	34.6
F	–	13.18	0.427	–1.670	0.019	0.013	0.05	–	–	–	–	–	–	–	–
1612-LCP :															
a	2	16.96	0.456	0.219	0.009	0.015	0.17	0.18	0.00	0.01	–0.00	–	0.0	–1.5	1.5
b	3	16.20	0.434	0.149	0.002	0.009	0.10	0.08	–0.00	0.01	–0.01	–	0.0	–14.1	14.1
c	6	13.33	0.340	-1.623	0.013	0.006	0.13	0.09	0.01	0.01	–0.03	–	0.0	–37.7	37.7
d	–	12.99	0.760	-1.594	0.014	0.009	0.09	–	–	–	–	–	–	–	–
1720-RCP :															
G	–	15.91	0.537	-0.333	0.004	0.004	7.71	–	–	–	–	–	–	–	–
H	–	14.99	0.531	-0.341	0.003	0.018	2.69	–	–	–	–	–	–	–	–
I	12	13.05	0.540	-0.341	0.012	0.011	5.25	2.86	0.20	–0.21	2.34	68	10.1	81.7	82.4
J	11	13.21	-1.578	-4.628	0.014	0.026	0.22	0.11	0.00	0.01	0.09	–	10.0	82.9	83.5
1720-LCP :															
e	8	15.10	0.547	-0.338	0.004	0.045	271.9	137.20	–4.43	1.70	–133.10	–34	3.5	–97.0	97.1
f	10	13.53	0.553	-0.348	0.021	0.005	5.98	3.75	–0.10	–0.11	–2.22	–68	3.9	–59.3	59.4
g	9	13.72	-1.559	-4.643	0.011	0.005	0.21	0.51	0.01	0.01	–0.05	–	3.5	–10.1	10.7

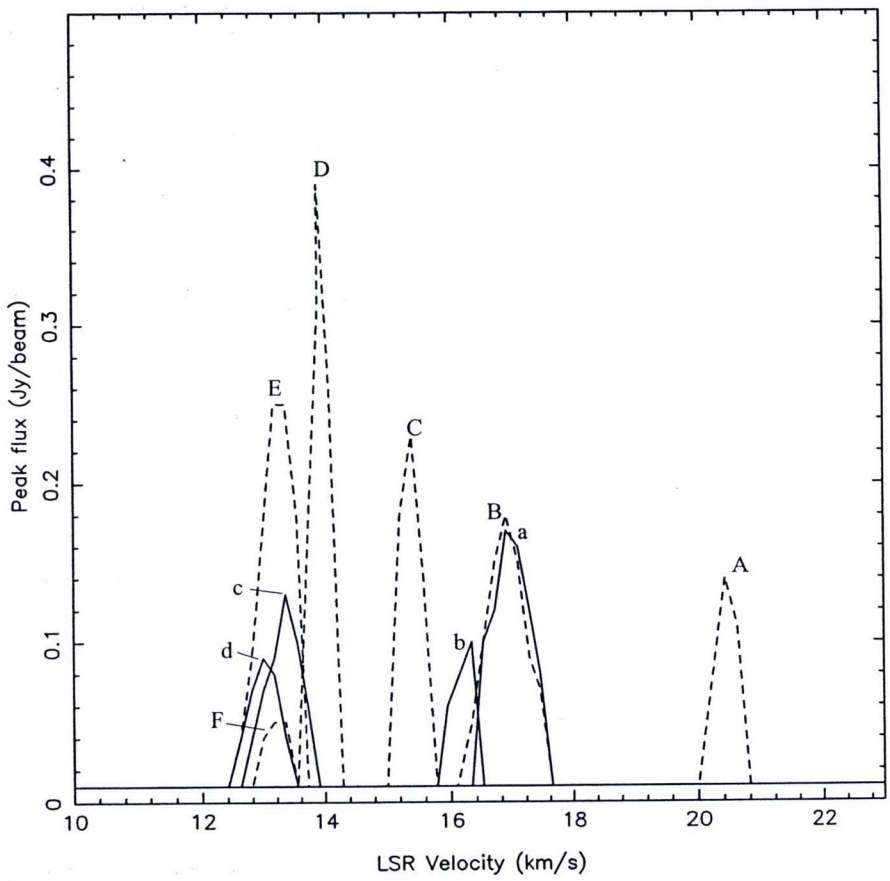

Figure 5.6 Velocity profiles of 1612 MHz OH masers in W49 S. Dash and solid lines are RCP and LCP respectively. The peak flux of each component is shown against the LSR velocity. The labeled features are listed in Table 5.1

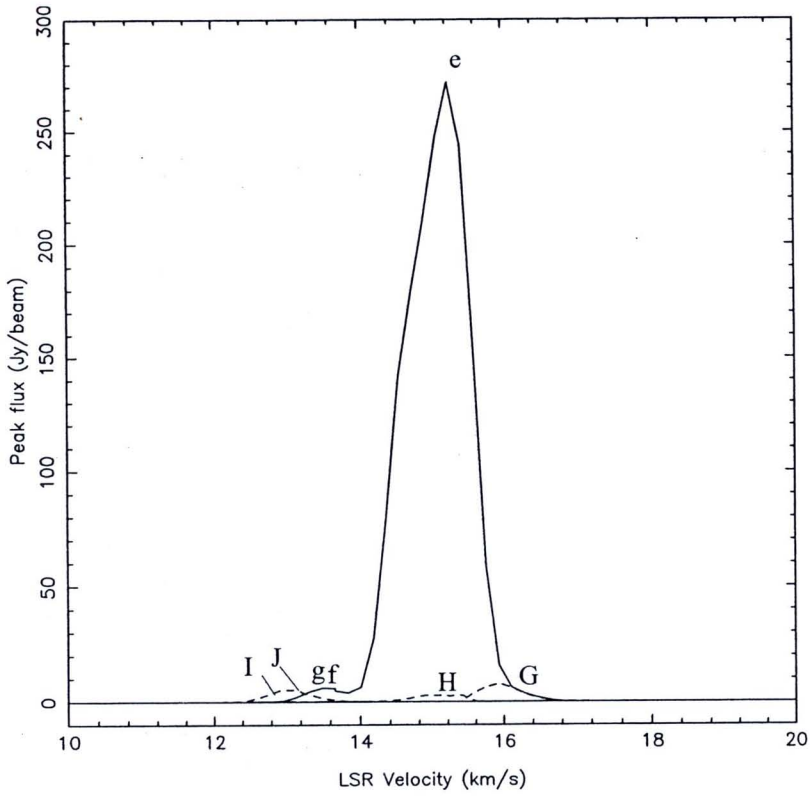

Figure 5.7 Velocity profiles of 1720 MHz OH masers in W49 S. Dash and solid lines are RCP and LCP respectively. The peak flux of each component is shown against the LSR velocity. The labeled features are listed in Table 5.1

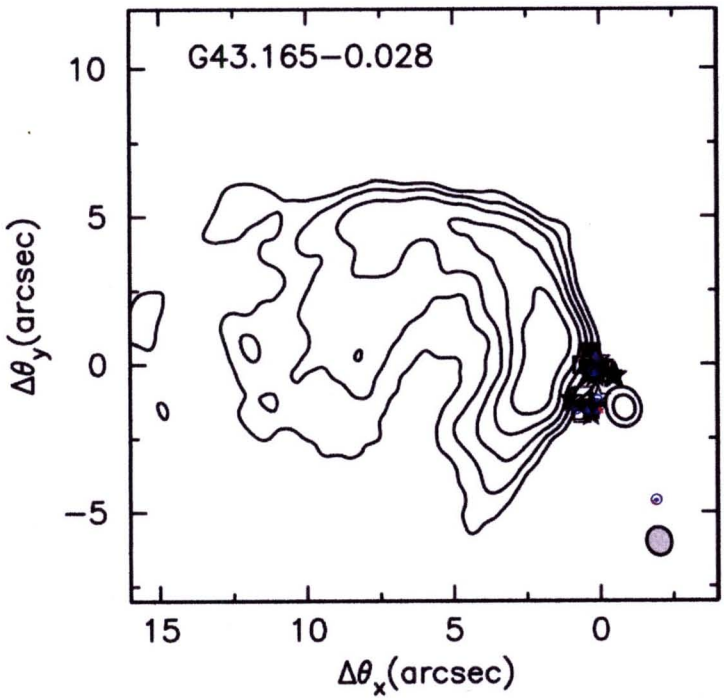

Figure 5.8 The positions of the1612 and 1720 MHz OH masers inW49 S from the MERLIN observations in 2005 May superimposed on the continuum VLA map at 8.4 GHz of the compact HII region,W49 S. The blue and red triangles represent the RCP and LCP of the 1612 MHz masers detected by MERLIN respectively, the corresponding circles representing the RCP and LCP of 1720 MHz masers. Other symbols show the masers detected by the VLA, with the 'stars' representing 1665, the 'squares' 1667 and the 'circles' 1720 MHz masers. Filled symbols are for LCP emission and unfilled symbols are for RCP emission.

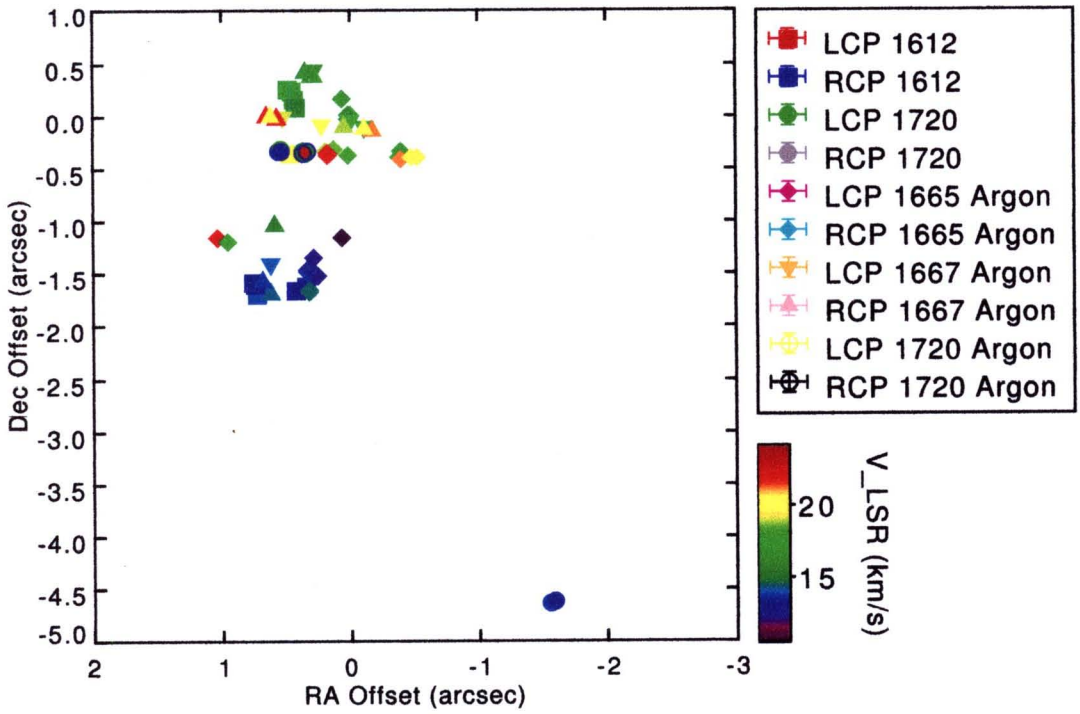

Figure 5.9 Positions and velocities of the 1612 and 1720 MHz OH masers from the MERLIN observations towardsW49 S compared with the results from Argon et al. (2000) where the data were obtained using the NRAO's VLA The colours show the LSR velocity (km s^{-1}). The positions are offset from (0,0) at R.A.(J2000)=$19^{h}10^{m}$ $21\overset{s}{.}65$, Dec.(J2000)=+09° 05′02″.6.

shown in Figure 5.10. One group of OH masers at (–1.6,–4.6) aresec has velocities between 13.21 and 13.72 km s^{-1}.

5.3.3 Polarization Properties of the Maser Features

Elliptical Gaussian components were fitted to components in the Stokes parameter, I, maps and their peak fluxes and positions measured. The fluxes in the corresponding Q, U and V maps were then measure at the positions of the peaks in the I maps. The polarised intensity flux (P) and the polarization position angle (PPA; χ) at the peak positions of the I components were also determined as described in Chapter 3 Section 3.7.5.

Table 5.2 shows the flux errors σ_I, σ_Q, σ_U, σ_V and σ_P obtained from the rms noise of each maser feature map. The errors in the position angles σ_χ), the percentage of linear (σ_{m_L}), circular (σ_{m_C}) and total (σ_{m_T}) polarization have been determined as described in 3 Section 3.7.5.

Figure 5.11 shows the percentage of circular polarization plotted against the

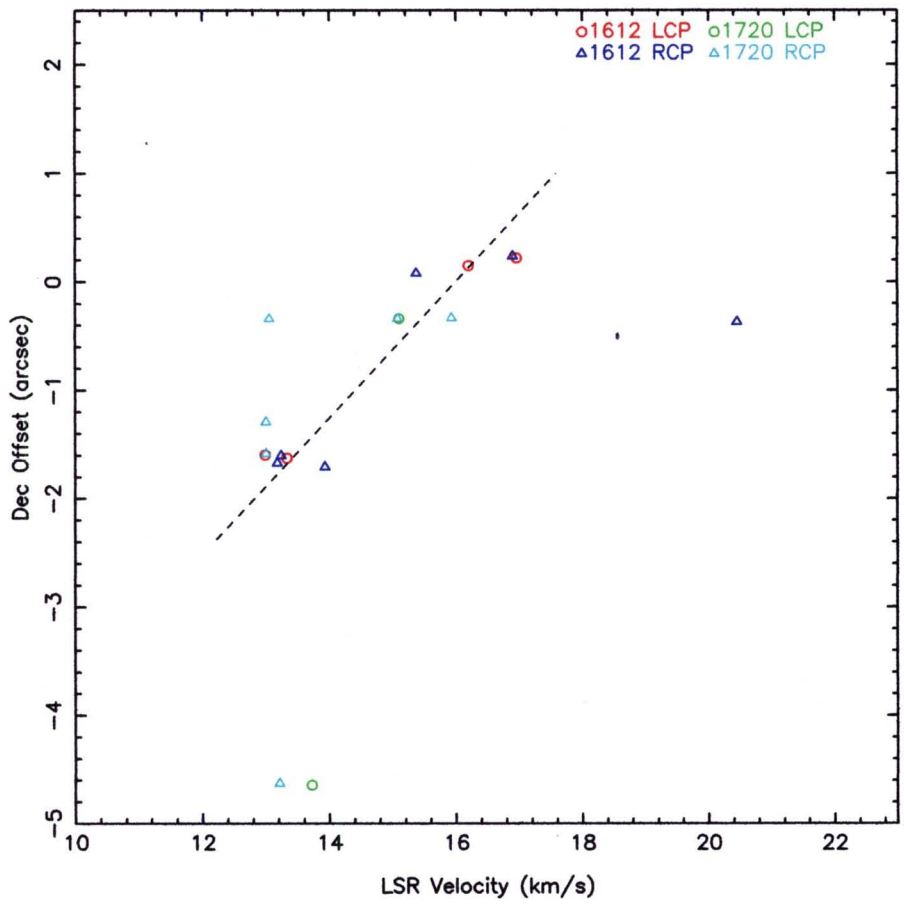

Figure 5.10 Plot of radial velocity against declination, for the OH 1612- and 1720-MHz masers in W49 S. The dashed line shows trending of the north–south velocity gradient.

percentage of linear polarization for both the 1612 and 1720 MHz maser features. For clarity, the overall statistics are shown in Figure 5.12. The left panel shows seven features with weak linear polarization (< 25%) and no features with strong linear polarization. Three features show strong circular polarization (> 75%). The right panel shows five features with weak linear polarization (< 25%). Two features show strong circular polarization (> 75%). In Table 5.2 features 2, 3, 6 and 7 have m_T<40% where these features have a low percentage of circular polarizations for 1612 MHz. Features 9 has the percentages of total polarization less than 11%. None of the linear polarization position angles have been measured at 1612 MHz. Three linear polarization position angles have been measured at 1720 MHz. They have values of –34°, –68° and +68°. Figure 5.11 and 5.12 show that linear polarization levels are generally very low compared with W75N and W3(OH). Possibly this might be caused by Faraday depolarization because of the large distance and high electron column density towards W49 A.

5.3.4 Magnetic fields

All LCP features can be identified as σ^- transitions from the Zeeman splitting of the OH maser emission as described in Chapter 3 Section 2.3.6. The RCP features can then be identified as σ^+. Four Zeeman pairs are shown in Table 5.3. The LCP features are matched so that they coincide to within the positional uncertainties with the identified I components. The magnetic field strengths have been determined from the velocity separation of the Zeeman pairs at 1612 and 1720 MHz by using a value for the velocity splitting of 0.236 km s^{-1} for a magnetic field strength of 1 mG (Davies, 1974). The field direction has been taken to be "Positive (+)" if the value of the velocity difference between the RCP and the LCP forming a Zeeman pair is positive and "negative (-)" if the difference is negative. The magnetic field strengths range from –2.0 to +2.2 mG, suggesting that the field is strong enough to be important for the star-formation process. The field strengths are the same level as measured in previous MERLIN observations of other star-forming regions. A comparison has been made with the magnetic field strengths determined by Fish et al. (2003), who obtained values of +1.5 mG at (0,0) arcsec for the head of the cometary region and +0.8 mG at (0.3,–1.5) arcsec (the southern clump). The MERLIN observations have resulted in values of –8.7 mG and +10.1 mG. The different magnetic field strengths need to be analysed further and comparisons made with other MERLIN observation lines.

Figure 5.13 shows the positions of the 1612 and 1720 MHz OH masers , the Zeeman pairs and the polarization information as listed in Table 5.3, which indicates that the two σ- components have very different polarization position angles (PPA; χ). According to the principles of the Zeeman effect, a Zeeman pair should have the same PPA in each feature. Gray et al. (2003) have suggested that a superposition of maser spots, not resolvable at the MERLIN resolution could result in very different projected field angles if the masers were to come from different depths in the disc. Therefore, it might be possible that feature numbers 8 and 12 (see Table 5.2) which have the PPAs of –34 and +68 degrees

Table 5.2 The error of flux, the polarization position angles, and the percentage of polarization of each OH maser feature in W49 S.

No.	Vel. (km s^{-1})	σ_I (Jy b^{-1})	σ_Q (Jy b^{-1})	σ_U (Jy b^{-1})	σ_V (Jy b^{-1})	σ_P (Jy b^{-1})	σ_χ (°)	σ_{m_L} (%)	σ_{m_C} (%)	σ_{m_T} (%)
				1612 MHz :						
1	20.42	<0.01	<0.01	<0.01	<0.01	0.00	0.00	0.0	18.3	18.28
2	16.88	<0.01	<0.01	<0.01	<0.01	0.00	0.00	0.0	−5.7	5.73
3	16.33	<0.01	<0.01	<0.01	<0.01	0.00	0.00	0.0	−13.3	13.25
4	15.40	<0.01	<0.01	<0.01	<0.01	0.00	0.00	0.0	11.2	11.22
5	13.91	<0.01	<0.01	<0.01	<0.01	0.00	0.00	0.0	6.6	6.64
6	13.35	<0.01	<0.01	<0.01	<0.01	0.00	0.00	0.0	−12.4	12.44
7	13.16	<0.01	<0.01	<0.01	<0.01	0.00	0.00	0.0	6.0	6.01
				1720 MHz :						
8	15.23	1.12	0.05	0.06	1.10	0.06	0.60	0.0	0.0	0.01
9	13.66	0.03	<0.01	<0.01	0.02	0.00	0.00	0.3	−0.3	0.41
10	13.49	0.03	<0.01	<0.01	0.02	0.00	0.00	0.4	0.5	0.57
11	13.14	0.02	<0.01	<0.01	<0.01	0.00	0.00	2.0	−2.0	2.8
12	12.96	0.03	<0.01	<0.01	0.02	0.00	0.00	8.9	11.5	14.5

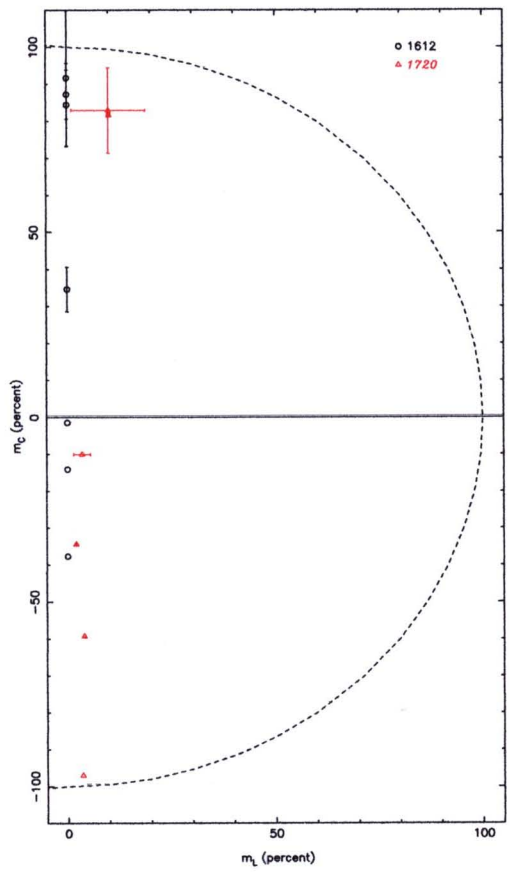

Figure 5.11 Percentage of linear(m_L) and circular polarization(m_C) of 1612 and 1720 MHz OH maser features in W49 S. Black and red colour are 1612 and 1720 MHz respectively. A completely polarised feature.[$m_T(\%) = (m_L^2+m_C^2)^{1/2} = 100\%$] will lie on the dotted line. Negative values of m_C comes from the negative values of the Stoke V.

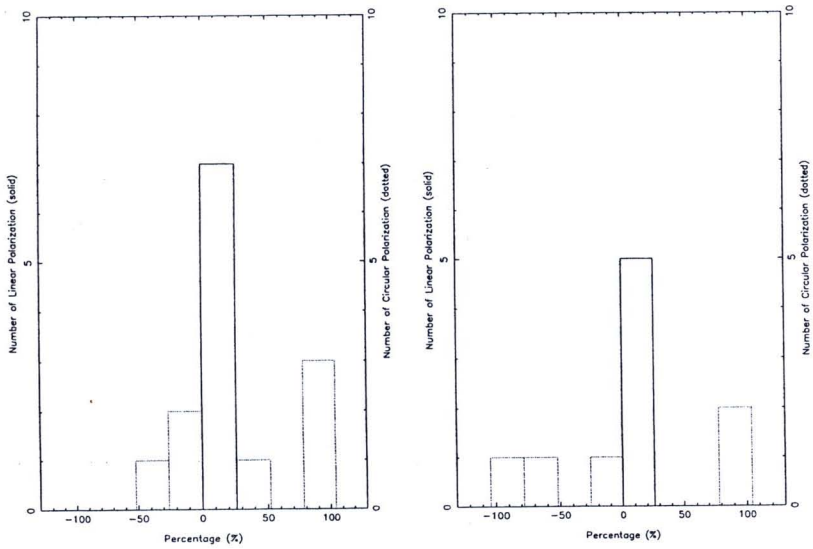

Figure 5.12 Histograms of percentage of linear and circular polarization of 1612 and 1720 MHz OH maser features in W49 S following Figure 5.11.

respectively, are the result of masers coming from different depths in the disc. Similarly for feature numbers 10 and 12 which have different the PPAs of –68 and +68 degrees respectively. It could also be that there are other factors involved in such cases; for example, a blending of OH masers at the same position plus Faraday rotation (Hutawarakorn and Cohen, 1999) in which the polarization properties of the emission grow as the masers propagate.

Figure 5.14, 5.15, 5.16 and 5.17 show the LCP, RCP, I, Q, U, V, the percentage of linear and circular polarization, and the measurable polarization position angles against velocity for the Zeeman pairs found at 1612 MHz and 1720 MHz. Zeeman pairs Z_1 and Z_2 show very strong peak fluxes for the Stokes LL, whereas Stokes RR fluxes profiles are quite weak as if they are blending at the same positions. This needs further investigation with a higher resolution telescope (e.g. VLBI) to clarify the real position of the masers.

5.4 W49 SW

The OH maser distribution in this region is presented in Section 5.4.1 and the associated kinematics are presented in Section 5.4.2. The polarization and magnetic fields of the maser features are presented in Section 5.4.3.

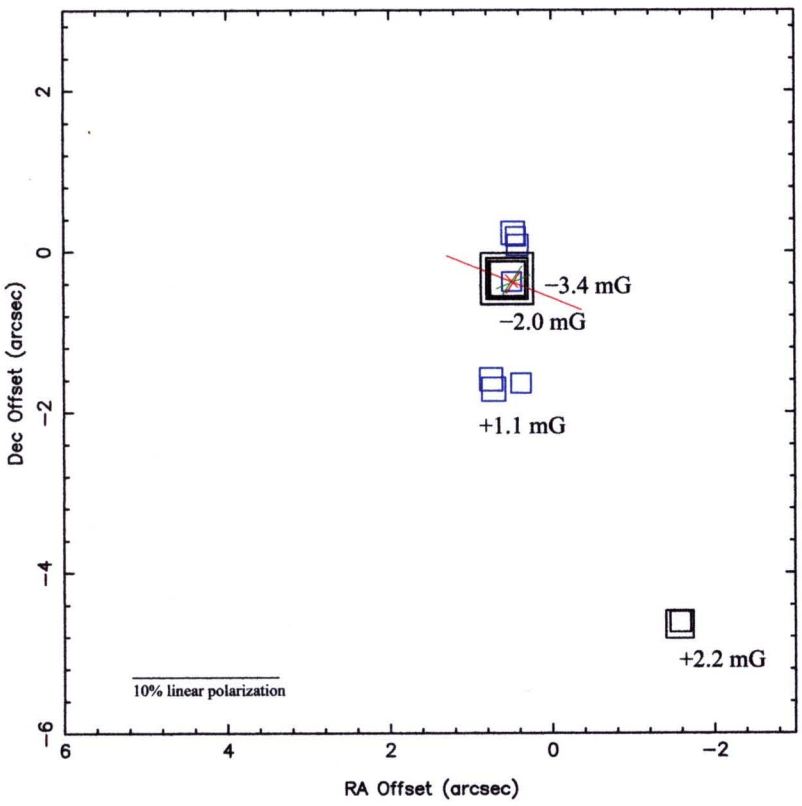

Figure 5.13 The 1612 and 1720 MHz OH maser features are shown with polarization information in W49 S. Blue and black colours are 1612 and 1720 MHz, respectively. The square area is proportional to the Stokes I flux of each feature. The vectors indicate the plane of the electric field vector and have lengths proportional to the percentage of linear polarization.

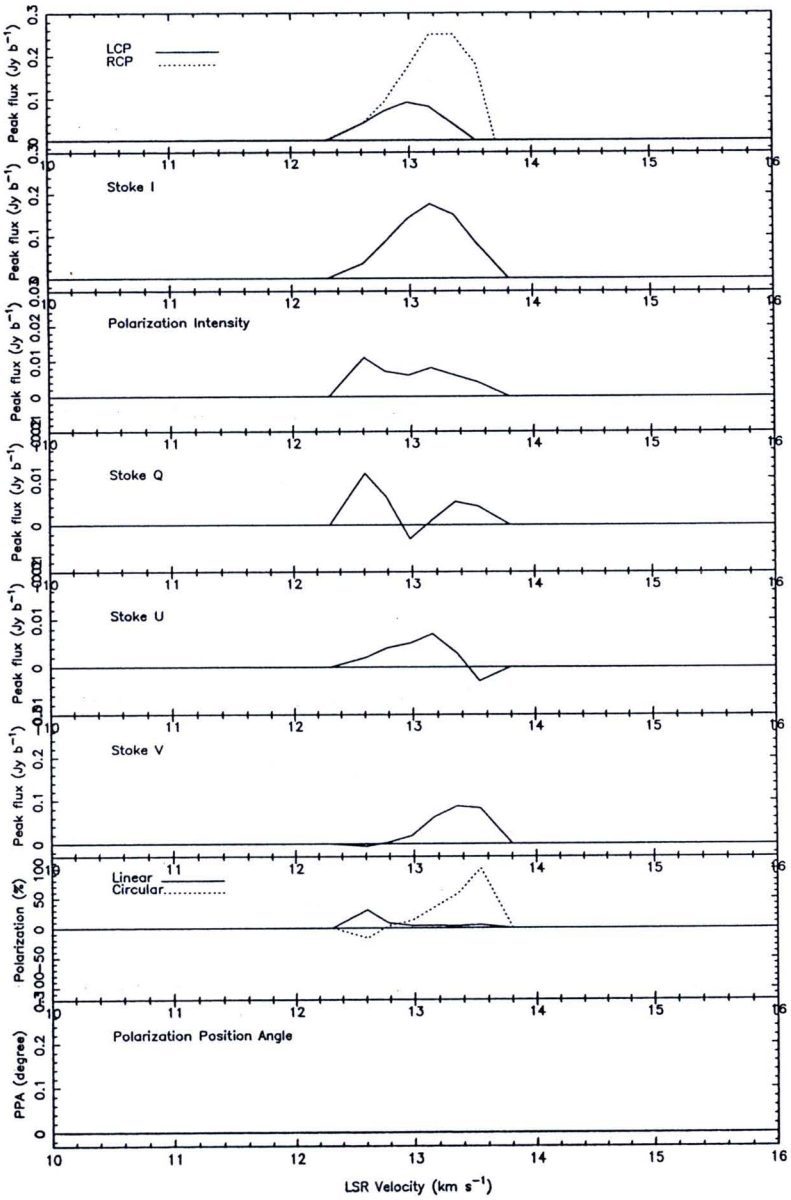

Figure 5.14 Velocity profiles of the Zeeman pair Z_1 at 1612 MHz in W49 S.

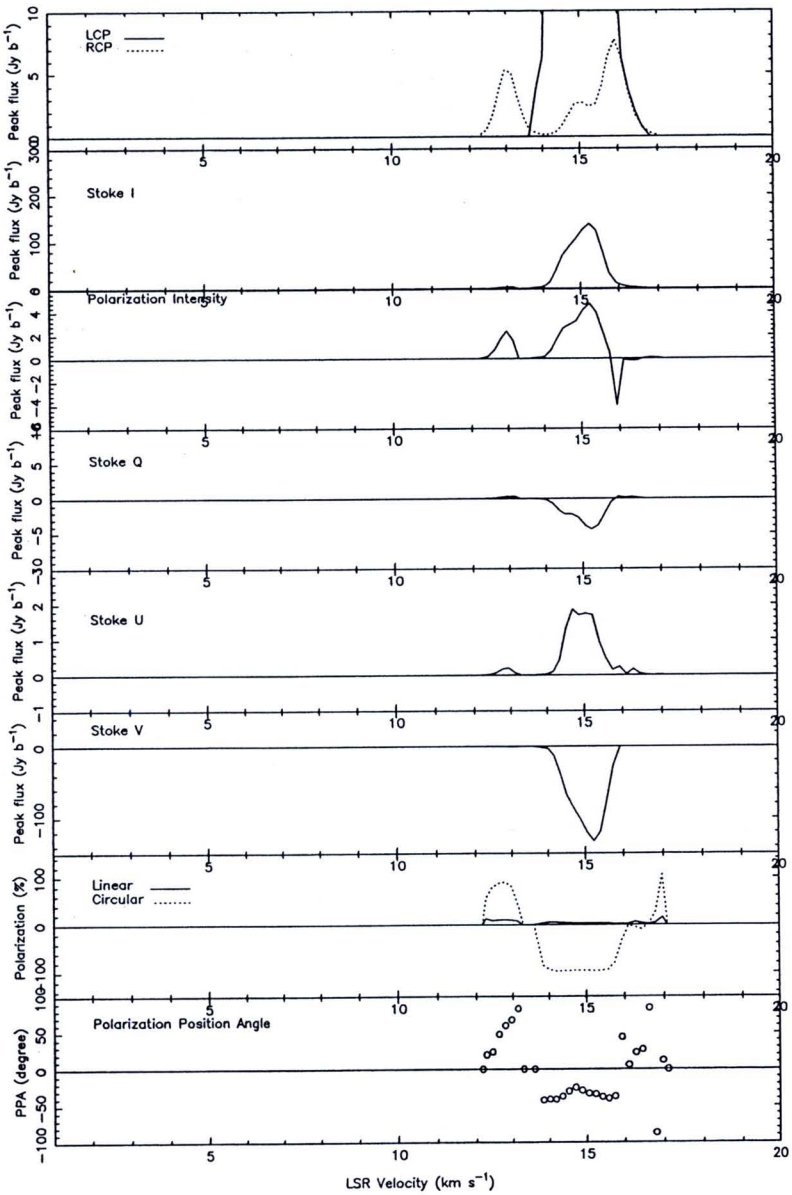

Figure 5.15 Velocity profiles of the Zeeman pair Z_1 at 1720 MHz in W49 S.

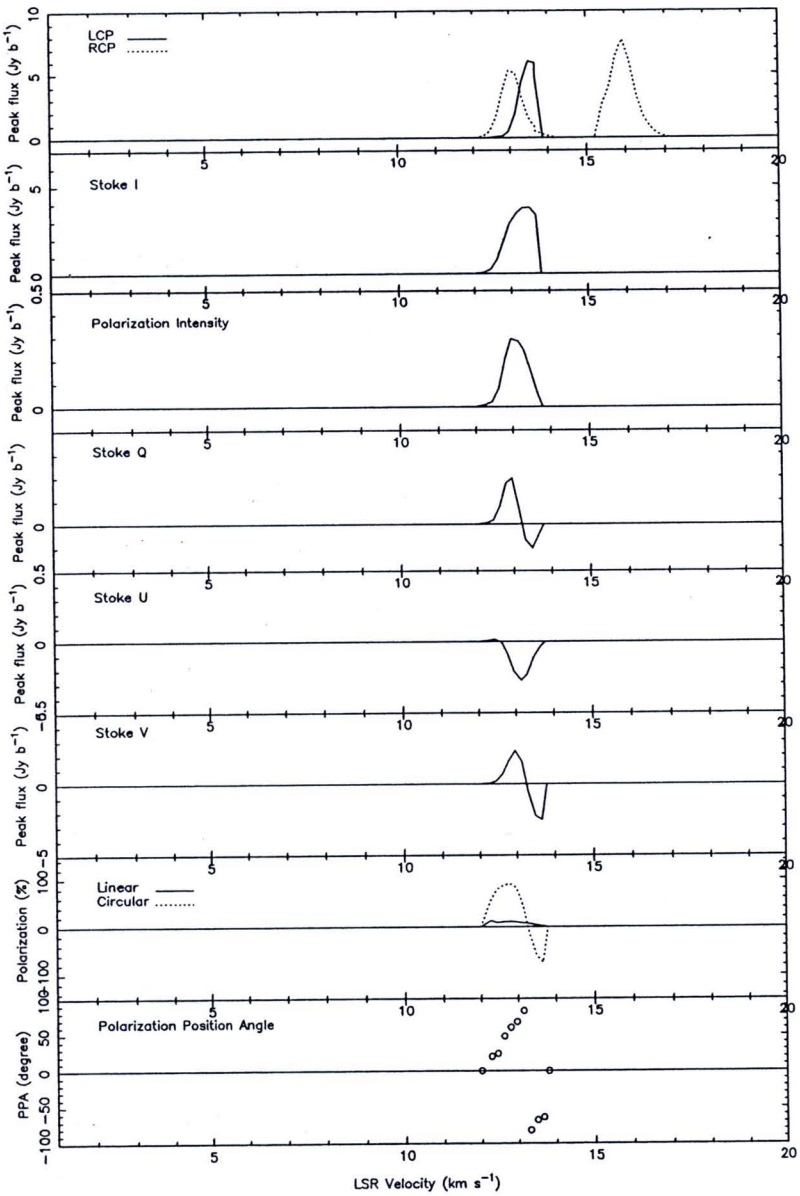

Figure 5.16 Velocity profiles of the Zeeman pair Z_2 at 1720 MHz in W49 S.

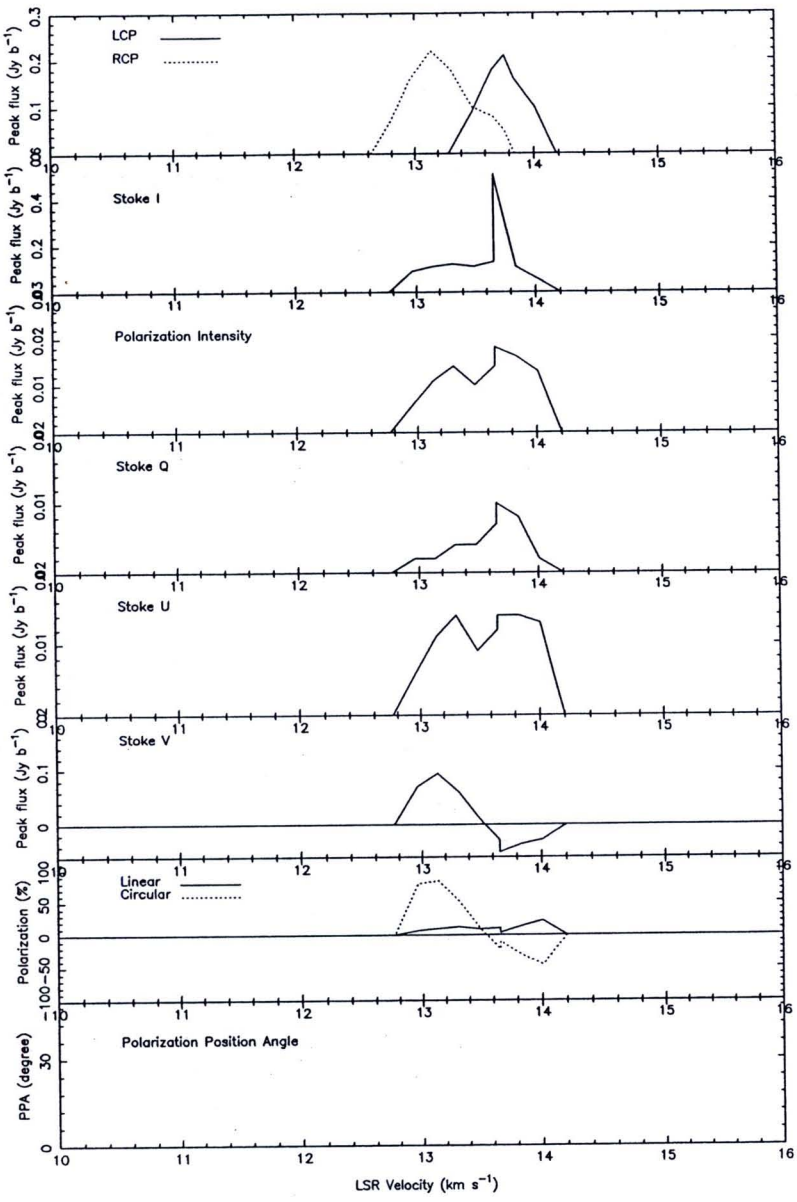

Figure 5.17 Velocity profiles of the Zeeman pair Z_3 at 1720 MHz in W49 S.

Table 5.3 Zeeman Pair Masers in W49 S.

Feature	I No.	Velocity (km/s)	RA offset (arcsec)	Dec offset (arcsec)	σ_{RA} (arcsec)	σ_{Dec} (arcsec)	Peak flux (Jy/beam)	B (mG)
				1612 MHz				
Z_1 :								
LCP-d	–	12.99	0.760	−1.594	0.014	0.009	0.09	+1.1
RCP-E	7	13.24	0.743	−1.603	0.005	0.017	0.25	
				1720 MHz				
possibility for Z_1 :								
LCP-e	8	15.10	0.547	−0.338	0.004	0.004	271.94	−3.4
RCP-G	–	15.91	0.537	−0.333	0.004	0.004	7.71	
RCP-H	–	14.99	0.531	−0.341	0.003	0.018	2.69	
RCP-I	12	13.05	0.540	−0.341	0.012	0.011	5.25	
possibility for Z_2 :								
LCP-f	10	13.53	0.553	−0.338	0.021	0.005	5.98	−2.0
RCP-G	–	15.91	0.537	−0.333	0.004	0.004	7.71	
RCP-H	–	14.99	0.531	−0.341	0.003	0.018	2.69	
RCP-I	12	13.05	0.540	−0.341	0.012	0.011	5.25	
Z_3 :								
LCP-g	9	13.72	−1.559	−4.643	0.011	0.005	0.21	+2.2
RCP-J	11	13.21	−1.578	−4.628	0.014	0.026	0.22	

5.4.1 OH Maser Distribution

The noise levels in the maps of the W49 SW sub-region are similar to those specified in Section 5.3.1. Table 5.4 gives the velocity, position, position uncertainty and peak flux density of each circularly polarised OH maser. The positional uncertainties in each feature are calculated from the standard deviation of the position of the components in that particular feature. The maps presented in Figure 5.19 - Figure 5.20 show positions relative to the pointing position labelled as the W49 region in Table 1 of Argon et al. (2000): R.A.(J2000)=$19^{\rm h}10^{\rm m}\ 11\overset{\rm s}{.}04$, Dec.(J2000)=+09° 05′ 20″.2. In this region there are only 2 different spectral line features, one in LCP and the other in RCP.

The velocity profiles of the 1720 MHz OH maser features are shown in Figure 5.18. Their emission extends from 12 to 14 km s^{-1}, and a comparison of their distribution with previous work (Argon et al. 2000) is shown in Figure 5.19. The OH masers at 1720 MHz could be associated with the 1667 MHz OH masers observed by Argon et al. (2000). All of the OH masers have a distribution similar to the ring shape around the regions Jl and J2 (see also the caption from Figure 15 of Argon et al. 2000).

5.4.2 OH Maser Kinematics

Figure 5.20 shows the position offset (from pointing position) and the velocity of each feature in both circular polarizations. The plot compares the current results with those taken from Argon et al. (2000). The OH masers seem to show red-shifted velocities on the left-hand side of the plot and blue-shifted on the right. This could be interpreted as OH masers tracing a rotating disc. Further analysis is needed to confirm this new finding.

Table 5.4 OH maser features in W49 SW. For each frequency and polarization, flux weighted mean velocities and positions are given for each feature. The positions are given relative to (0,0) at R.A.(J2000)=$19^{h}10^{m}11^{s}.04$, Dec.(J2000)=+09° 05′20″.2.

Feature	Stoke no.	Vel. (km/s)	RA offset (arcsec)	Dec offset (arcsec)	σ_{RA} (arcsec)	σ_{Dec} (arcsec)	Peak flux (Jy b^{-1})	I (Jy b^{-1})	Q (Jy b^{-1})	U (Jy b^{-1})	V (Jy b^{-1})	PA °	M_L (%)	M_C (%)	M_T (%)
1720-RCP :															
M	**13**	13.57	-1.585	-2.675	0.027	0.013	0.14	0.05	0.01	0.01	0.07	–	28.0	148.2	150.8
1720-LCP :															
h	**14**	12.83	-1.554	-2.681	0.005	0.002	0.35	0.17	–0.01	0.01	–0.16	–	6.7	–97.8	98.0

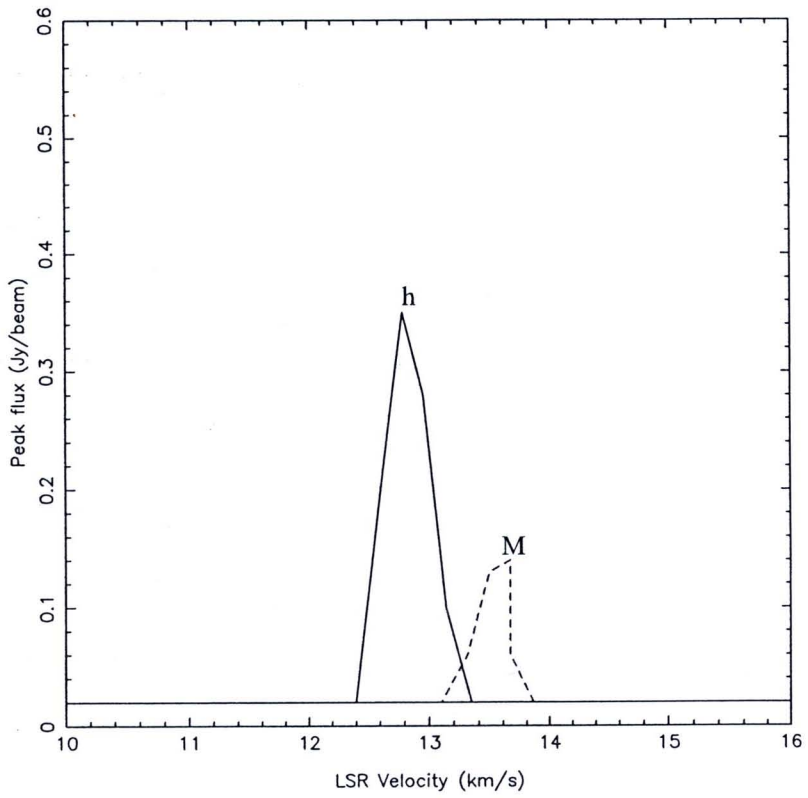

Figure 5.18 Velocity profiles of 1720 MHz OH masers in W49 SW. Dash and solid lines are RCP and LCP respectively. The peak flux of each component is shown against the LSR velocity. The labeled features are listed in Table 5.4

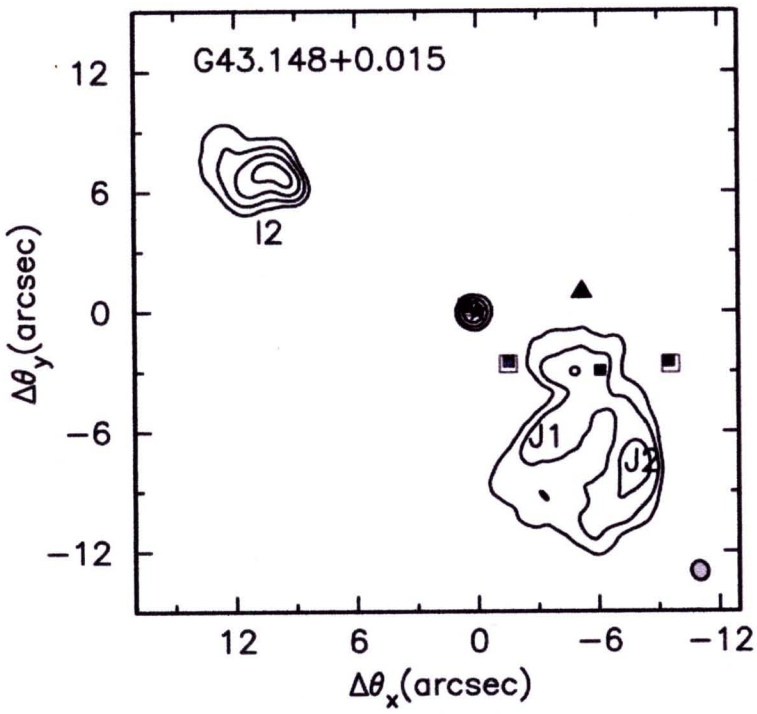

Figure 5.19 The positions of 1720 MHz OH masers in W49 SW with MERLIN observation in 2005 May superimpose on the continuum VLA map at 8.4 GHz of compact HII region W49 SW. The Components I2, J1, and J2 are labeled in the upper plot (Wink et al., 1975). See Figure 5.8 caption for details.

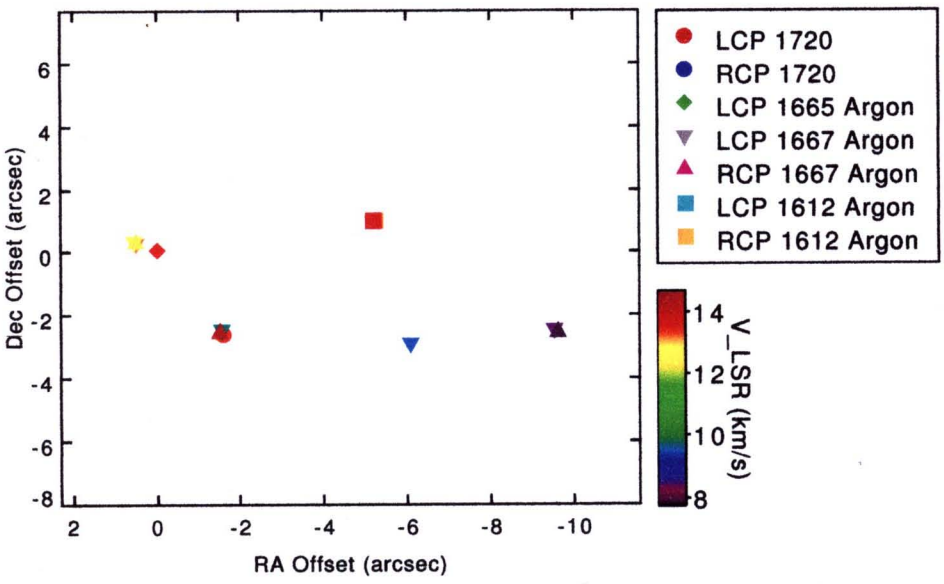

Figure 5.20 Positions and velocities of the 1720 MHz OH masers from MERLIN observations towards W49 SW compare with the results from Argon et al. (2000) where the data were obtained by VLA of NRAO. The colours show the radial velocity (km s^{-1}). The positions are offset from (0,0) at R.A.(J2000)=$19^{h}10^{m}11\overset{s}{.}04$, Dec.(J2000)=+09° 05′20″.2.

5.4.3 Polarization Properties and Magnetic Field

The flux errors σ_I, σ_Q, σ_U, σ_V and σ_P obtained from the rms noise of the channel maps are given in Table 5.5. The errors in the position angles (σ_χ), the percentage of linear (σ_{m_L}), circular (σ_{m_C}) and total (σ_{m_T}) polarization have been determined as described in Chapter 3 Section 3.7.5. Figure 5.21 also shows the distribution of the percentages of linear and circular polarization of the 1720 MHz features. Both features (13 & 14) exhibit pure circular polarization ($m_C > 90\%$).

No polarization position angle could be observed from this region (see Figure 5.22). Only one Zeeman pair (Z_1) was found in the region at 1720 MHz, details of which are presented in Table 5.6. The velocity profile of this Zeeman pair is shown in Figure 5.23. It exhibits strong circular polarization, implying a magnetic field strength of 3.1 mG in a direction towards the observer. Fish et al. (2003) obtained a value +3.0 mG for the magnetic field at a position (–6,+1) arcsec, whereas the MERLIN value is –3.1 mG at a position (–1.6,–2.8) arcsec. This can be interpreted as a field reversal in W49 SW, which supports the velocity distribution as seen in Figure 5.20. Further analysis is needed to confirm this new finding.

5.5 W49 N

The OH maser distribution in this region is presented in Section 5.5.1 and the associated kinematics are presented in Section 5.5.2. The polarization of the maser features are presented in Section 5.5.3. Magnetic fields derived from Zeeman measurements are presented in Section 5.5.4.

5.5.1 OH Maser Distribution

The noise levels in the maps of the W49 N sub-region are similar to those specified in Section 5.3.1. Table 5.7 gives the velocity, position, position uncertainty and peak flux density of each circularly polarised OH maser. The positional uncertainties in each feature have been calculated from the standard deviation of the positions of the components in that particular feature. The maps presented show positions relative to the pointing position labelled as the W49 N region in Table 1 of Argon et al. (2000): R.A.(J2000)=$19^{\rm h}10^{\rm m}13\overset{\rm s}{.}18$, Dec.(J2000)=+09°06′ 12″.2.

In this region there are 21 different spectral line features, ten of which are seen in LCP and eleven in RCP. The velocity profiles of the 1720 MHz OH maser features are shown in Figure 5.24. Their emission extends widely from –3 to 33 km s^{-1}. In fact, this is wider than previously detected by Argon et al. (2000), probably because of the higher sensitivity of the MERLIN measurements.

Figure 5.25 shows the positions of the 1720 MHz OH maser features found in these observations, superimposed on the 8.4 GHz continuum map by Argon et al. (2000). The black symbols represent the results from previous work and the

Table 5.5 The error of flux, the polarization position angles, and the percentage of polarization of each OH maser feature in W49 SW.

No.	Vel. (km s^{-1})	σ_I (Jy b^{-1})	σ_Q (Jy b^{-1})	σ_U (Jy b^{-1})	σ_V (Jy b^{-1})	σ_P (Jy b^{-1})	σ_χ (°)	σ_{m_L} (%)	σ_{m_C} (%)	σ_{m_T} (%)
				1720 MHz :						
13	13.66	<0.01	<0.01	<0.01	<0.01	0.00	0.00	0.0	30.6	30.6
14	12.79	<0.01	<0.01	<0.01	<0.01	0.00	0.00	0.0	–8.4	8.4

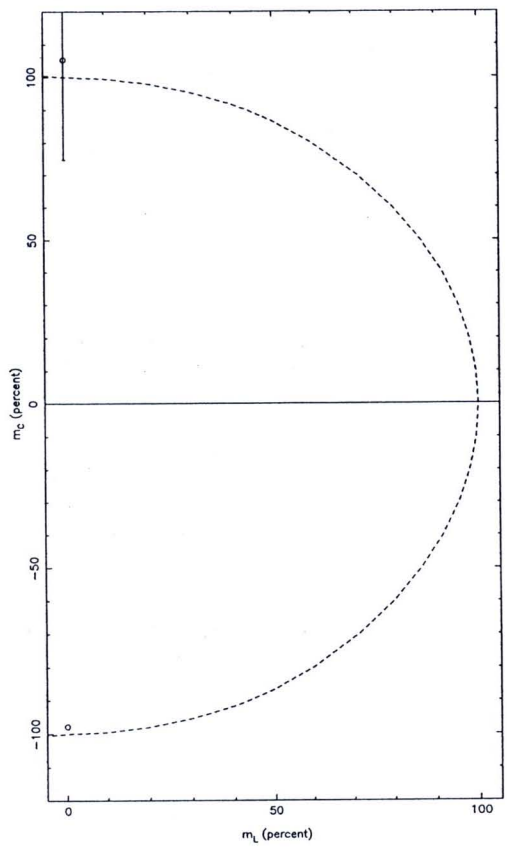

Figure 5.21 Percentage of linear(m_L) and circular polarization(m_C) of 1720 MHz OH maser features in W49 SW. A completely polarised feature.[$m_T(\%) = (m_L^2 + m_C^2)^{1/2} = 100\%$] will lie on the dotted line. Negative values of m_C comes from the negative values of the Stoke V.

Table 5.6 Zeeman Pair Masers in W49 SW.

Feature	I No.	Velocity (km/s)	RA offset (arcsec)	Dcc offset (arcsec)	σ_{RA} (arcsec)	σ_{Dec} (arcsec)	Peak flux (Jy/beam)	B (mG)
				1720 MHz				
Z_1 :								
LCP-h	14	12.83	−1.554	−2.681	0.005	0.002	0.35	−3.1
RCP-M	13	13.57	−1.585	−2.675	0.027	0.013	0.14	

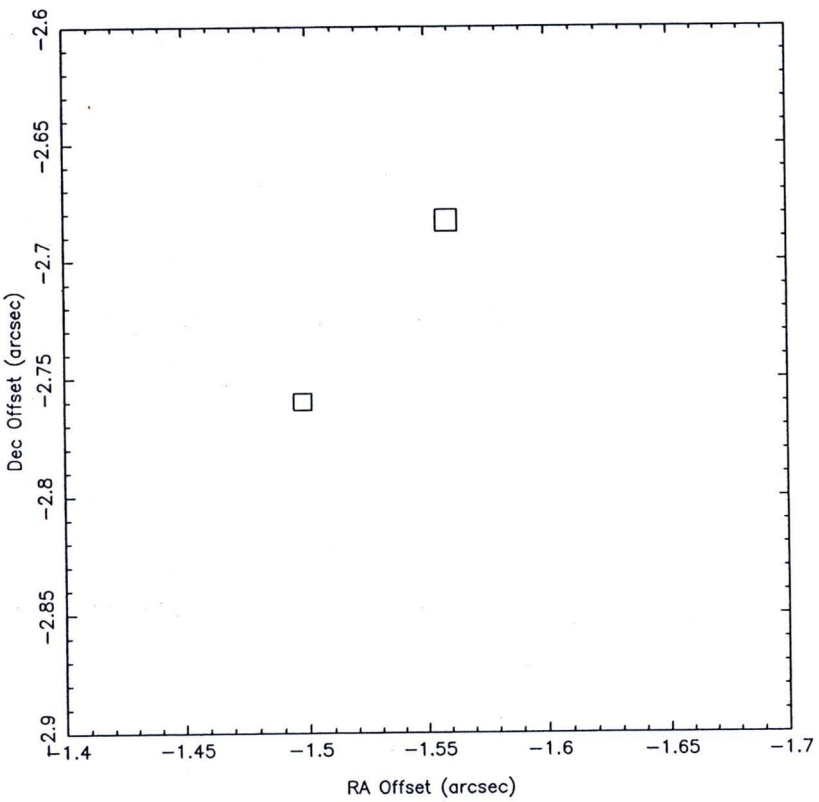

Figure 5.22 The 1720 MHz OH maser features are shown with polarization information in W49 SW. The square area is proportional to the Stokes I flux of each feature.

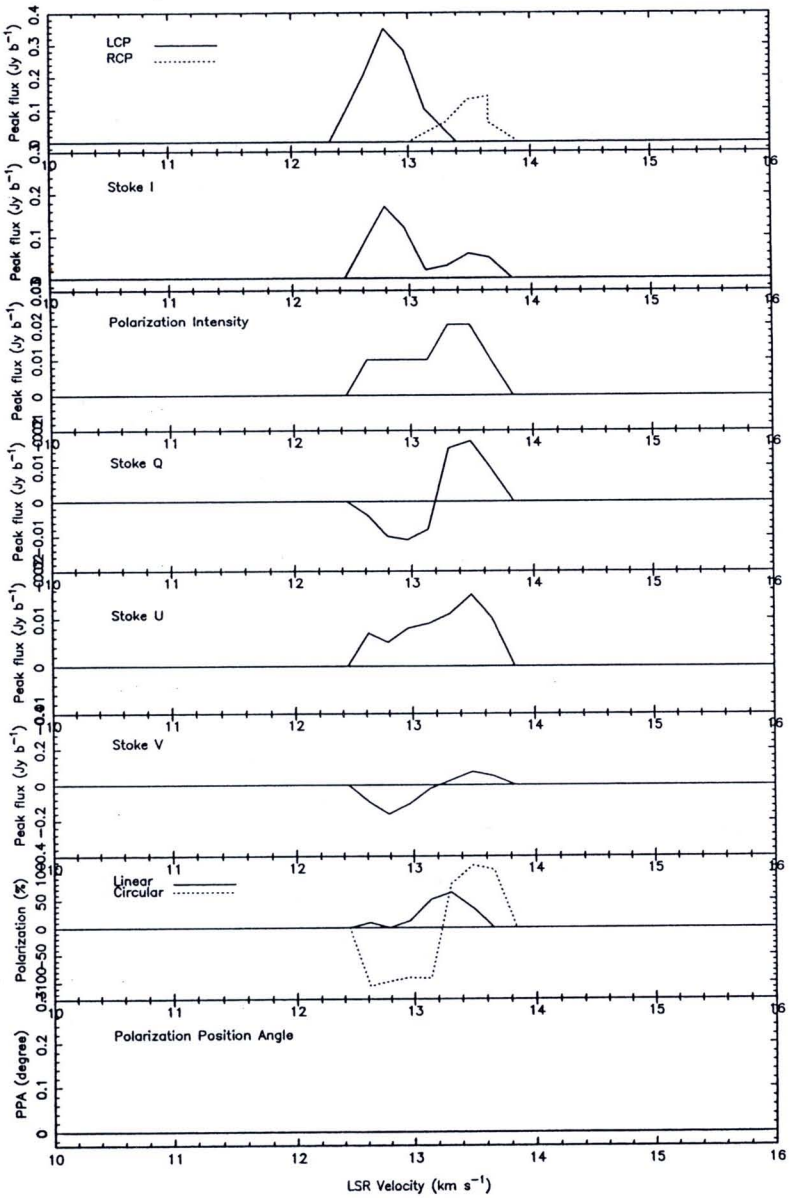

Figure 5.23 Velocity profiles of the Zeeman pair Z_1 at 1720 MHz in W49 SW.

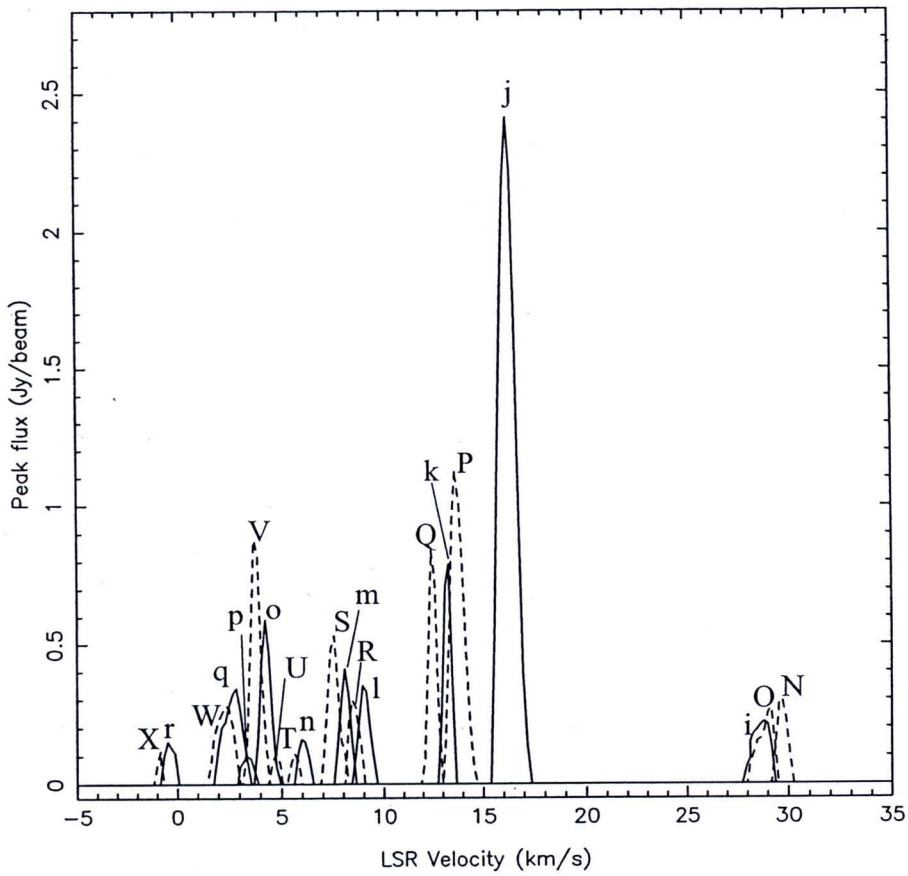

Figure 5.24 Velocity profiles of 1720 MHz OH masers in W49 N. Dash and solid lines are RCP and LCP, respectively. The peak flux of each component is shown against the LSR velocity. The labeled features are listed in Table 5.7

current results are represented by the blue- and red-coloured circle symbols. The OH masers are located mainly at or close to regions B and B1. There is also a group associated with region F to the north, and another group on the limb of region A which has been defined as a bipolar outflow source. There do not appear to be any OH masers at 1720 MHz associated with the ultra-compact region, G. This implies that the OH masers are located in a cooler area outside the ultra-compact region. Finally, there is a group in an easterly direction, which might be associated with another group near region J.

Table 5.7 OH maser features in W49 N. For each frequency and polarization, flux weighted mean velocities and positions are given for each feature. The positions are given relative to (0,0) at R.A.(J2000)=$19^h10^m\ 13\overset{s}{.}18$, Dec.(J2000)=+09° 06′12″.2.

Feature	Stoke no.	Velocity (km/s)	RA offset (arcsec)	Dec offset (arcsec)	σ_{RA} (arcsec)	σ_{Dec} (arcsec)	Peak flux (Jy/beam)	I (Jy/beam)	Q (Jy/beam)	U (Jy/beam)	V (Jy/beam)	PA °	M_L (%)	M_C (%)	M_T (%)
1720-RCP :															
N	15	29.71	–0.372	1.205	0.011	0.004	0.30	0.14	0.00	0.01	0.14	–	5.7	100.9	101.0
O	16	28.99	–0.368	1.186	0.028	0.024	0.27	0.18	0.01	–0.00	0.07	–	4.4	35.3	35.6
P	18	13.71	–4.799	1.707	0.002	0.010	1.13	0.57	0.02	0.00	0.54	42	3.6	94.5	94.6
Q	20	12.49	0.807	2.890	0.006	0.008	0.84	0.42	0.01	–0.02	0.40	79	5.5	95.4	95.5
R	22	8.51	10.039	1.237	0.004	0.007	0.30	0.21	0.01	–0.00	0.08	–	0.0	39.5	39.5
S	24	7.51	9.949	1.228	0.018	0.015	0.53	0.28	0.01	–0.00	0.25	–	0.0	87.9	87.9
T	26	5.66	3.122	11.524	0.021	0.019	0.11	0.07	–0.01	0.00	0.02	–	0.0	24.4	24.4
U	–	4.75	–0.313	0.069	0.009	0.005	0.11	–	–	–	–	–	–	–	–
V	28	3.80	3.439	10.095	0.010	0.006	0.88	0.46	0.03	–0.01	0.41	52	7.2	90.1	90.4
W	31	2.30	3.174	11.169	0.015	0.006	0.28	0.24	–0.01	0.00	0.03	–41	0.0	12.9	12.9
X	33	-0.85	1.907	2.577	0.012	0.012	0.12	0.06	–0.00	–0.02	0.05	–	0.0	98.5	98.5
1720-LCP :															
i	–	28.65	–0.368	1.181	0.020	0.019	0.22	–	–	–	–	–	–	–	–
j	17	16.26	–4.792	1.700	0.009	0.006	2.41	1.09	–0.05	0.02	–1.02	–35	4.8	–93.6	93.7
k	19	13.25	0.823	2.888	0.001	0.001	0.79	0.36	–0.01	0.01	–0.34	–	0.0	–94.8	94.8
l	21	9.03	10.037	1.237	0.008	0.008	0.35	0.19	0.01	0.00	–0.12	–	0.0	–61.1	61.1
m	23	8.09	9.950	1.211	0.003	0.008	0.41	0.22	–0.01	–0.00	–0.10	–	0.0	–47.1	47.1
n	25	6.06	3.159	11.531	0.013	0.015	0.16	0.06	–0.01	–0.01	–0.04	–	0.0	–67.5	67.5
o	27	4.27	3.471	10.086	0.004	0.009	0.59	0.34	–0.02	–0.01	–0.19	–52	6.1	–56.7	57.1
p	29	3.37	0.073	–0.318	0.029	0.024	0.10	0.06	0.00	–0.00	–0.03	–	0.0	–43.5	43.5
q	30	2.69	3.194	11.167	0.015	0.013	0.34	0.19	–0.01	0.01	–0.10	–21	0.0	–54.0	54.0
r	32	–0.38	1.949	2.548	0.005	0.009	0.15	0.05	–0.01	–0.00	–0.04	–	0.0	–89.3	89.3

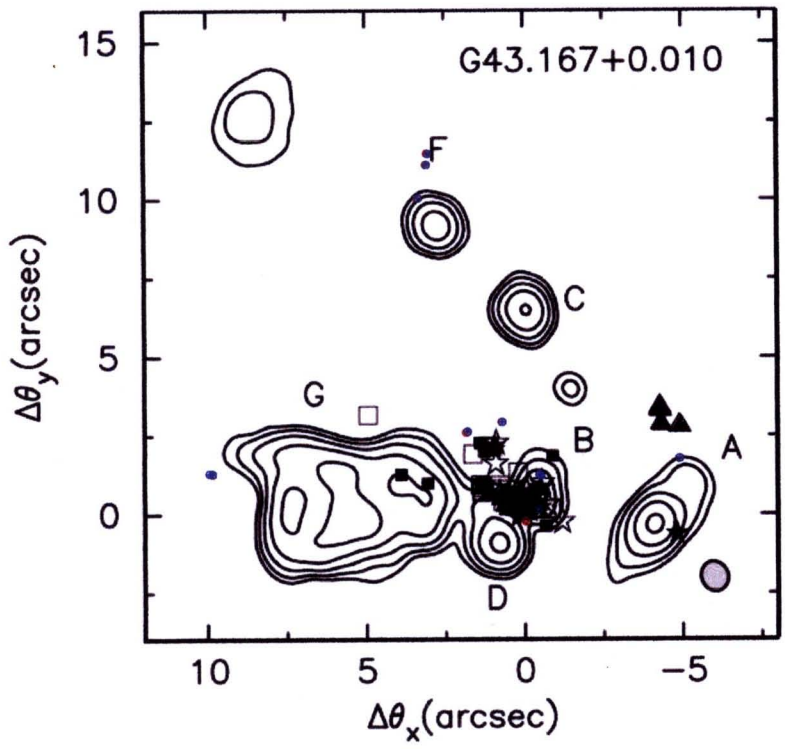

Figure 5.25 The positions of 1720 MHz OH masers in W49 N with MERLIN observation in 2005 May superimpose on the continuum VLA map at 8.4 GHz of compact HII region W49 N. See Figure 5.8 caption for details.

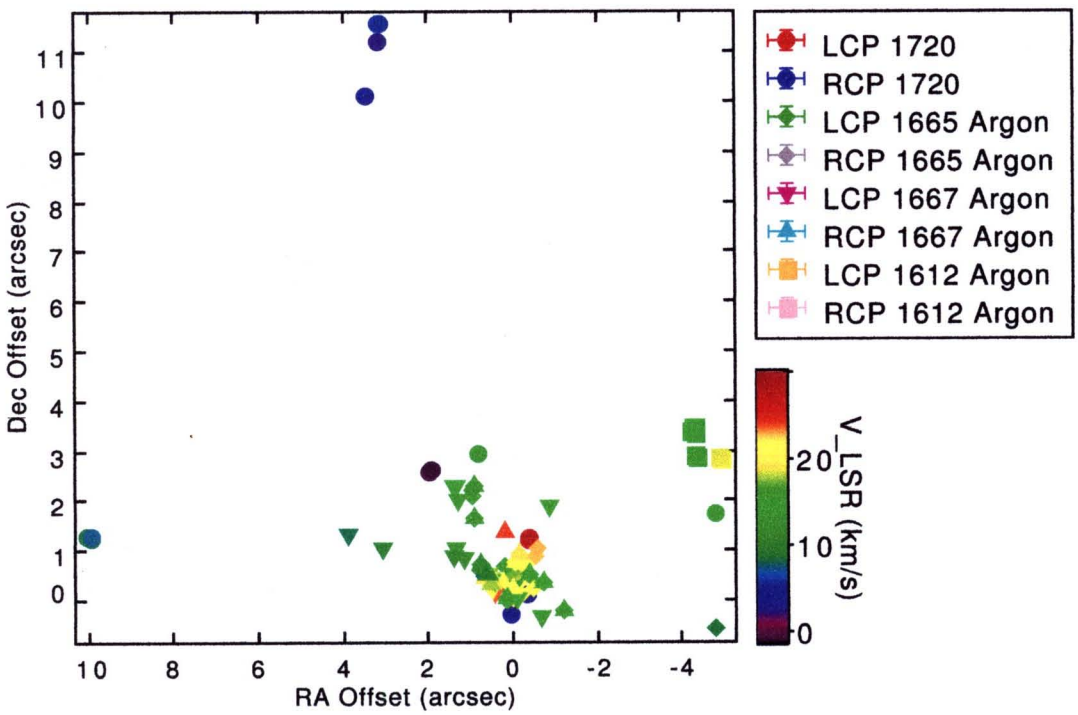

Figure 5.26 Positions and velocities of the 1720 MHz OH masers from MERLIN observations towards W49 N compare with the results from Argon et al. (2000) where the data were obtained by VLA of NRAO. The colours show the LSR velocity (km s^{-1}). The positions are given relative to (0,0) at R.A.(J2000)=$19^h10^m13\overset{s}{.}18$, Dec.(J2000)=+09° 06′12″.2.

5.5.2 OH Maser Kinematics

The positions and velocities of the 1720 MHz masers are plotted in Figure 5.26. The maser group at region F has a velocity gradient from +6.06 to +2.30 km s^{-1} in a north to south direction. The group in region A has velocities between +12.83 and +13.57 km s^{-1}, but shows no evidence of bipolar outflow. However, in the centre of region B there are masers with red- shifted velocities between +28.65 and +29.31 km s^{-1} in a south-westerly direction and blue- shifted ones between –0.38 and –0.85 km s-1 to the north-east. A CO outflow model, proposed by Smith et al. (2009) has the strongest water masers in the centre of region G. The model shows a blue-shifted wing to the southeast and a red-shifted one to the northwest (as shown in Figure 5.3). Some of the OH masers velocities in this region are associated with both red-shifted and blue-shifted velocities. However, further analysis is required to confirm this result. It is to be noticed that the velocities of the water and OH masers are clearly separated in position as shown in Figure 5.2. This behaviour can be understood if the water and OH masers arise in completely different environments.

5.5.3 Polarization Properties of the Maser Features

The flux errors σ_I, σ_Q, σ_U, σ_V and σ_P obtained from the rms noise of the channel maps are given in Table 5.8. The errors in the position angles σ_χ), the percentage of linear (σ_{m_L}), circular (σ_{m_C}) and total (σ_{m_T}) polarization have been determined as described in Chapter 3 Section 3.7.5. Figure 5.27 also shows the distribution of the percentages of linear and circular polarization of the 1720 MHz features. For clarity, overall statistics are shown in Figure 5.28. All of the maser features have weak linear polarization (< 40%). Ten features show strong circular polarization (> 75%). The values for the percentages of circular polarization vary widely, which is similar to the results found for W49 S. This might be caused by Faraday depolarization because of the large distance and high electron column density towards W49 A. In Table 5.8 features 31 exhibits weak circular polarization. Five linear polarization position angles were measured from the 1720 MHz data. They have values of +42°, +52°, +78°, −36° and −52°.

5.5.4 Magnetic Fields

Table 5.9 shows the details of the identified Zeeman pairs and Figure 5.29 shows the positions of the 1720 MHz OH masers with their polarization information, and identifying the Zeeman pairs listed in Table 5.9. In W49 N, four Zeeman pairs have been identified and gave values of −2.2, −1.7, +1.4 and +10.8 mG for the magnetic field. The minus and plus symbols indicate the field directions 'towards' and 'away' from the observer respectively. (Sarma et al., 2002) have determined the strength of the magnetic field from the water masers in region G. They found a field reversal close to region G, which is in agreement with the OH 1720 MHz maser observations with MERLIN.

Figure 5.30, 5.31, 5.32 and 5.33 show the velocity profiles for those Zeeman pairs found at 1720 MHz in LCP, RCP, I, Q, U, V, the percentage of linear and circular polarization, and the measured polarization position angles. The Zeeman pair, Z_2, shows a variation in the polarization position angle from 0 to 60° across the feature. This would need further investigation to see whether the variations are caused by a combination of bulk motions in the maser zone or arise from the physical processes associated with the maser amplification.

5.6 Summary

In addition to the already known masers in the W49 A molecular cloud complex, a number of new OH masers have also been detected. New 1612 and 1720 MHz OH masers have been detected in the sub-regions W49 N and W49 S. A reversal of the magnetic fields in W49 SW, W49 N and W49 S have also been found, which will very useful for constraining future theoretical models.

Table 5.8 The error of flux, the polarization position angles, and the percentage of polarization of each OH maser feature in W49 N.

No.	Vel. km s^{-1}	σ_I (Jy b^{-1})	σ_Q (Jy b^{-1})	σ_U (Jy b^{-1})	σ_V (Jy b^{-1})	σ_P (Jy b^{-1})	σ_χ (°)	σ_{m_L} (%)	σ_{m_C} (%)	σ_{m_T} (%)
				1720 MHz :						
15	29.70	<0.01	<0.01	<0.01	<0.01	0.00	0.00	0.0	10.1	10.14
16	29.18	<0.01	<0.01	<0.01	<0.01	0.00	0.00	0.0	5.8	5.8
17	16.28	<0.01	<0.01	<0.01	<0.01	0.00	0.00	0.9	−1.3	1.56
18	13.66	<0.01	<0.01	<0.01	<0.01	0.00	0.00	1.7	2.4	2.97
19	13.31	<0.01	<0.01	<0.01	<0.01	0.00	0.00	0.0	−3.9	3.86
20	12.44	<0.01	<0.01	<0.01	<0.01	0.00	0.00	2.4	3.3	4.02
21	8.95	<0.01	<0.01	<0.01	<0.01	0.00	0.00	0.0	−6.0	6.03
22	8.43	<0.01	<0.01	<0.01	<0.01	0.00	0.00	0.0	5.2	5.22
23	8.08	<0.01	<0.01	<0.01	<0.01	0.00	0.00	0.0	−5.0	5.01
24	7.56	<0.01	<0.01	<0.01	<0.01	0.00	0.00	0.0	4.7	4.72
25	5.99	<0.01	<0.01	<0.01	<0.01	0.00	0.00	0.0	−19.1	19.05
26	5.64	<0.01	<0.01	<0.01	<0.01	0.00	0.00	0.0	14.0	13.98
27	4.25	<0.01	<0.01	<0.01	<0.01	0.00	0.00	3.0	−3.4	4.53
28	3.72	<0.01	<0.01	<0.01	<0.01	0.00	0.00	2.2	2.9	3.67
29	3.37	<0.01	<0.01	<0.01	<0.01	0.00	0.00	0.0	−18.4	18.36
30	2.85	<0.01	<0.01	<0.01	<0.01	0.00	0.00	0.0	−5.9	5.95
31	2.33	<0.01	<0.01	<0.01	<0.01	0.00	0.00	0.0	4.2	4.21
32	−0.46	<0.01	<0.01	<0.01	<0.01	0.00	0.00	0.0	−27.8	27.79
33	−0.81	<0.01	<0.01	<0.01	<0.01	0.00	0.00	0.0	25.4	25.45

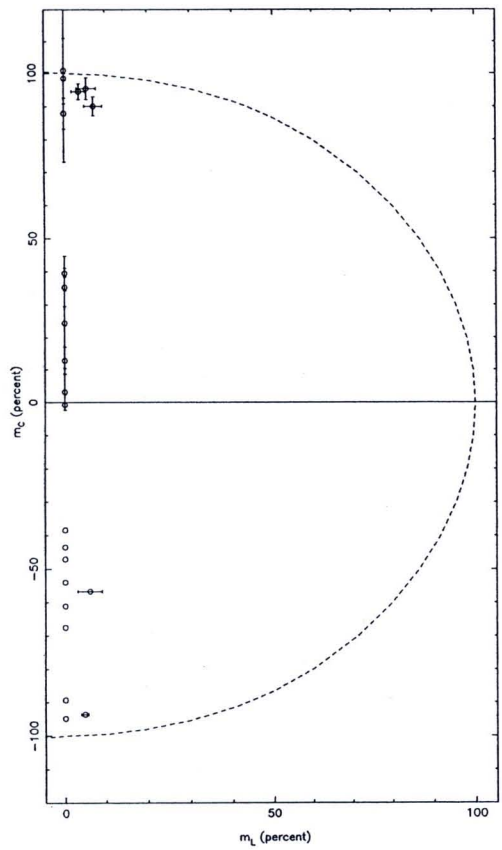

Figure 5.27 Percentage of linear(m_L) and circular polarization(m_C) of 1720 MHz OH maser features in W49 N. A completely polarised feature.[$m_T(\%) = (m_L^2 + m_C^2)^{1/2} = 100\%$] will lie on the dotted line. Negative values of m_C comes from the negative values of the Stoke V.

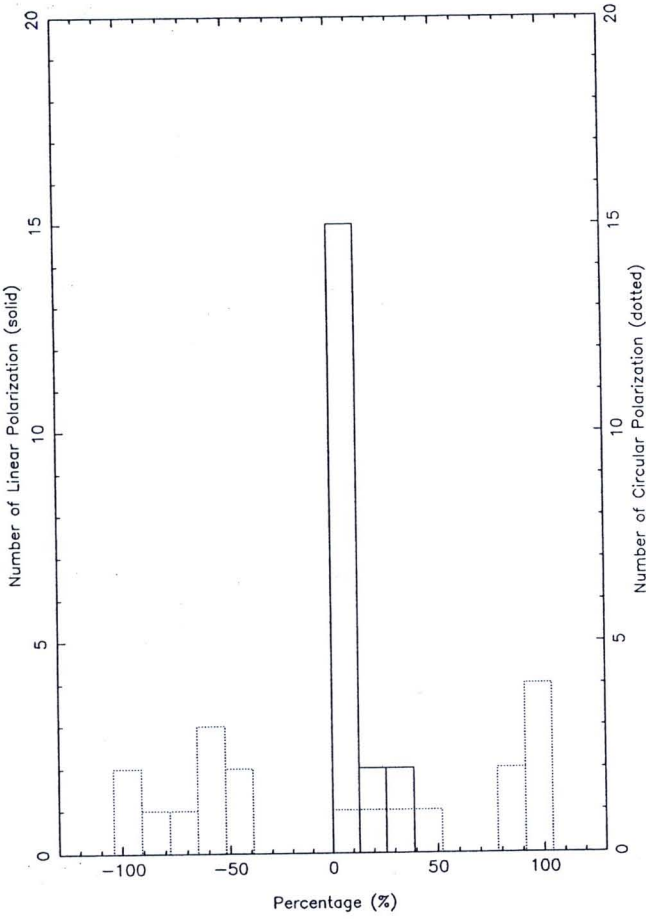

Figure 5.28 Histograms of percentage of linear and circular polarization of 1720 MHz OH maser features in W49 N following Figure 5.27.

Table 5.9 Zeeman Pair Masers in W49 N.

Feature	I No.	Velocity (km/s)	RA offset (arcsec)	Dec offset (arcsec)	σ_{RA} (arcsec)	σ_{Dec} (arcsec)	Peak flux (Jy/beam)	B (mG)
				1720 MHz				
Z_1 :								
LCP-i	–	28.65	−0.368	1.181	0.020	0.019	0.22	+1.4
RCP-O	16	28.99	−0.368	1.186	0.028	0.024	0.27	
Z_2 :								
LCP-j	17	16.26	−4.792	1.700	0.009	0.006	2.41	+10.8
RCP-P	18	13.71	−4.799	1.707	0.002	0.010	13.71	
Z_3 :								
LCP-l	21	9.03	10.037	1.237	0.008	0.008	0.35	−2.2
RCP-R	22	8.51	10.039	1.237	0.004	0.007	0.30	
Z_4 :								
LCP-q	30	2.69	3.194	11.167	0.015	0.013	0.34	−1.7
RCP-W	31	2.30	3.174	11.169	0.015	0.006	0.28	

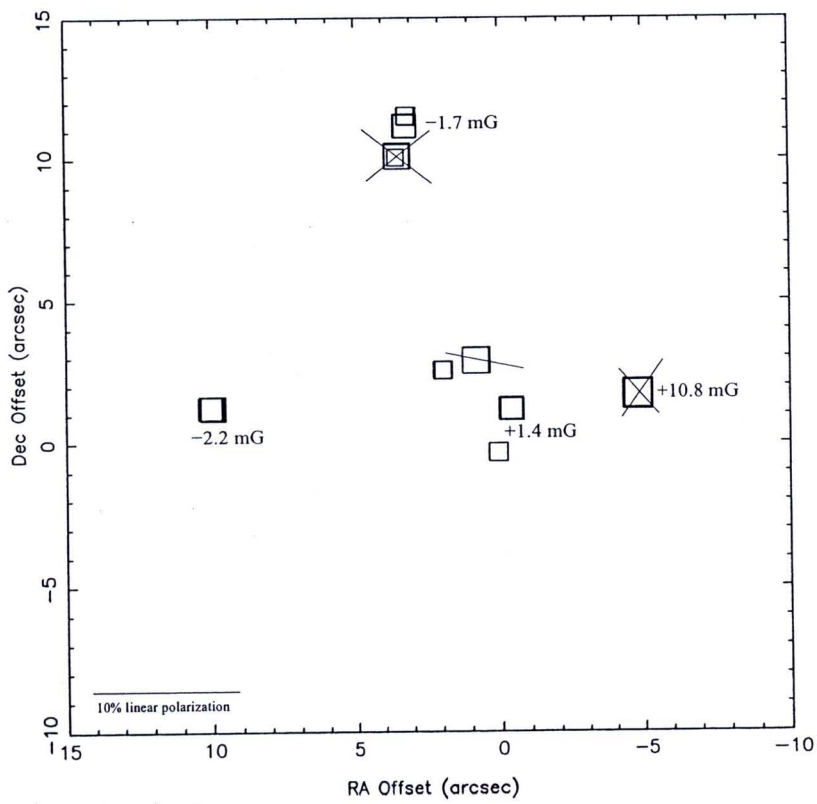

Figure 5.29 The 1720 MHz OH maser features are shown with polarization information in W49 N. The square area is proportional to the Stokes I flux of each feature. The vectors indicate the plane of the electric field vector and have lengths proportional to the percentage of linear polarization.

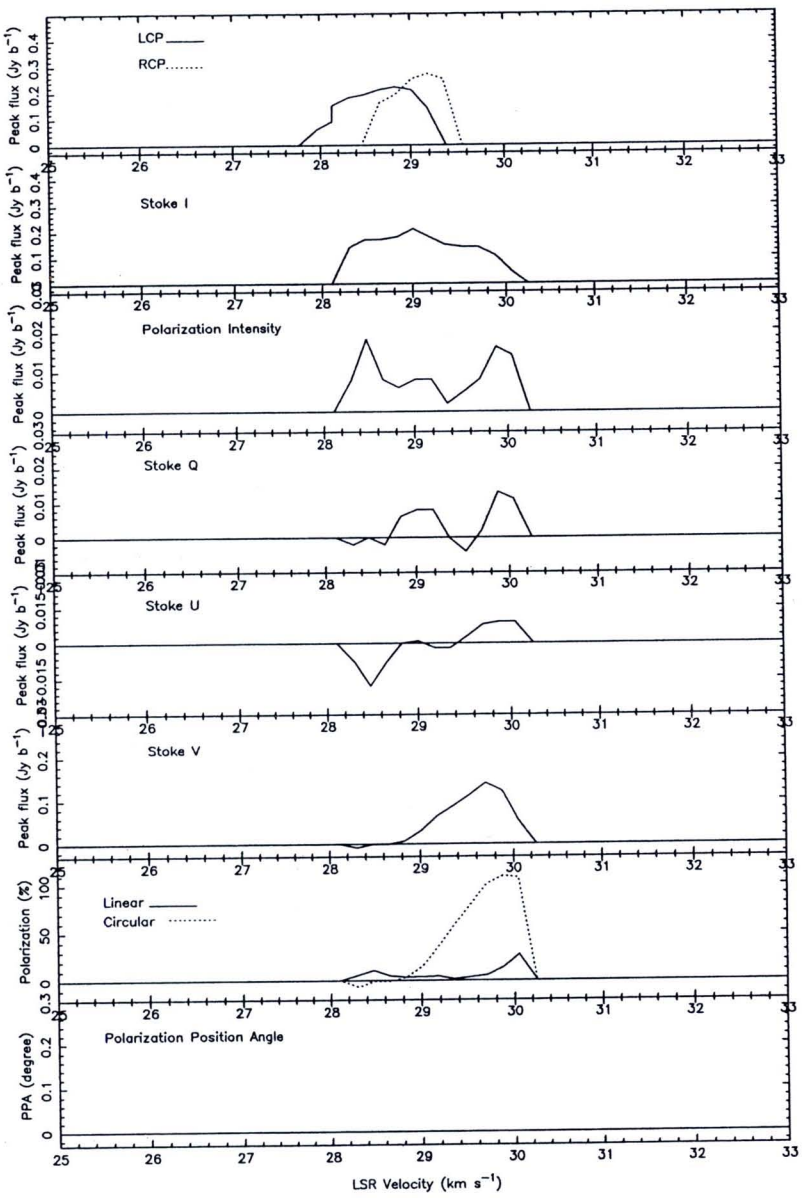

Figure 5.30 Velocity profiles of the Zeeman pair Z_1 at 1720 MHz in W49 N.

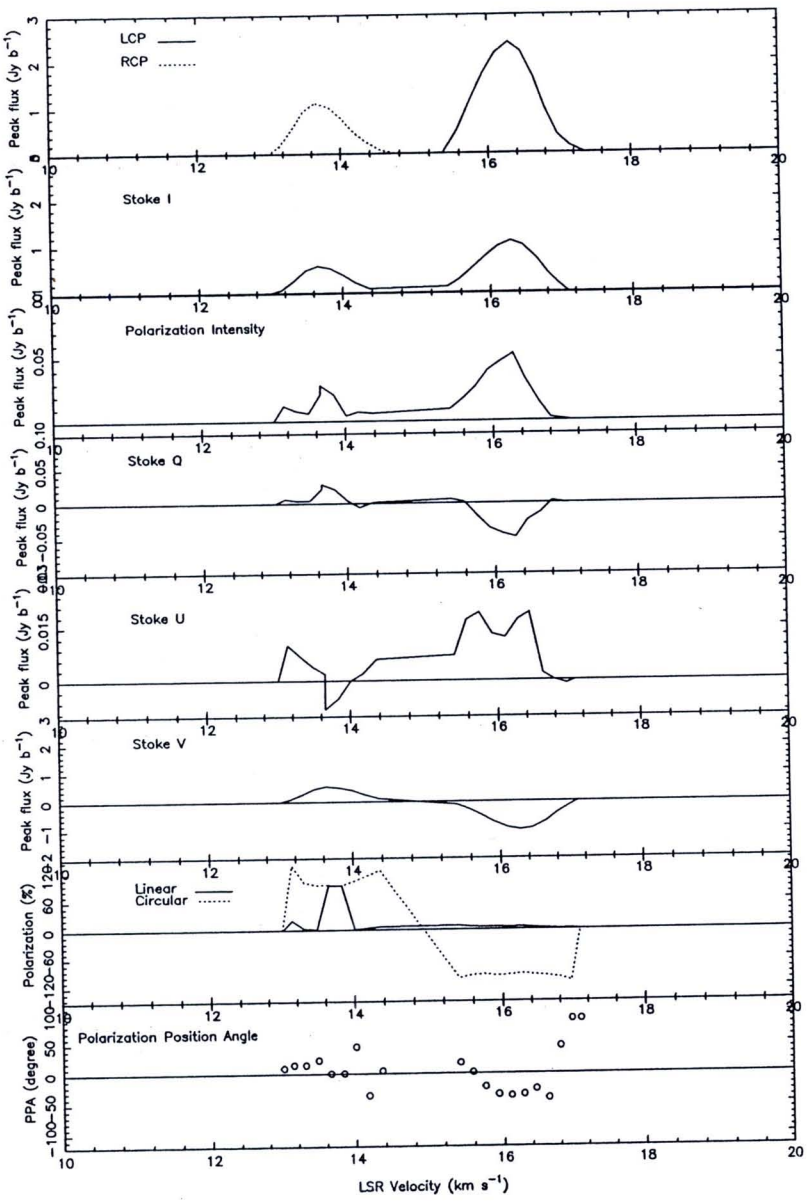

Figure 5.31 Velocity profiles of the Zeeman pair Z_2 at 1720 MHz in W49 N.

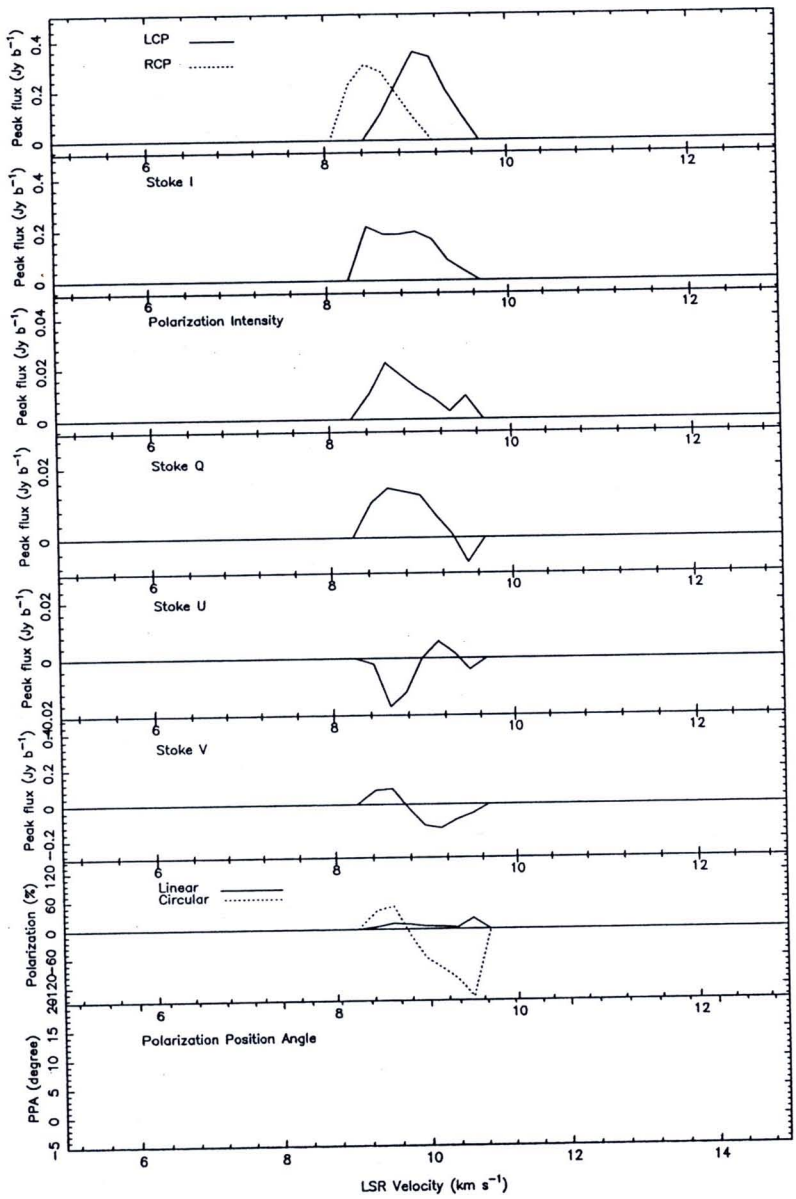

Figure 5.32 Velocity profiles of the Zeeman pair Z_3 at 1720 MHz in W49 N.

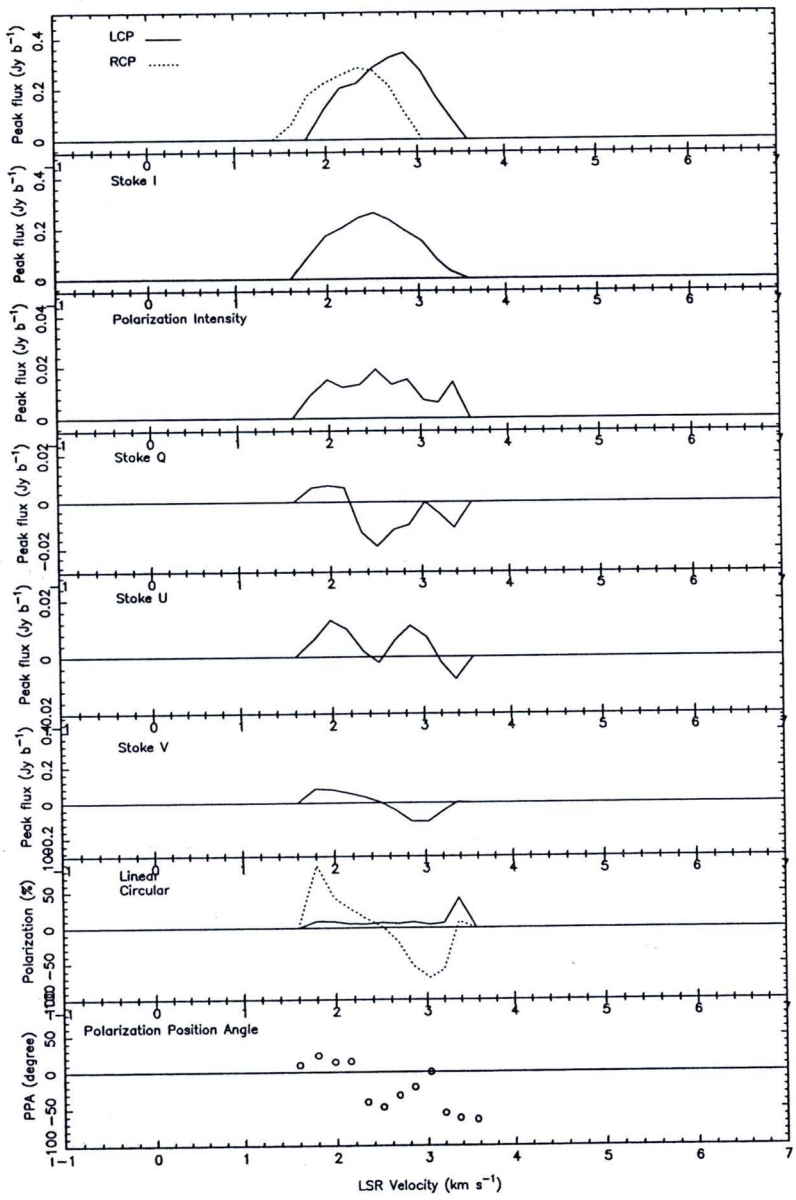

Figure 5.33 Velocity profiles of the Zeeman pair Z_4 at 1720 MHz in W49 N.